

# Nfat and miR-25 cooperate to reactivate the transcription factor Hand2 in heart failure

Ellen Dirkx<sup>1,13</sup>, Monika M. Gladka<sup>1,13</sup>, Leonne E. Philippen<sup>1</sup>, Anne-Sophie Armand<sup>2</sup>, Virginie Kinet<sup>1</sup>, Stefanos Leptidis<sup>1,3</sup>, Hamid el Azzouzi<sup>1,3</sup>, Kanita Salic<sup>1,3</sup>, Meriem Bourajja<sup>3</sup>, Gustavo J. J. da Silva<sup>4</sup>, Servé Olieslagers<sup>1</sup>, Roel van der Nagel<sup>5</sup>, Roel de Weger<sup>6</sup>, Nicole Bitsch<sup>1</sup>, Natasja Kisters<sup>1</sup>, Sandrine Seyen<sup>1</sup>, Yuka Morikawa<sup>7</sup>, Christophe Chanoine<sup>2</sup>, Stephane Heymans<sup>1</sup>, Paul G. A. Volders<sup>1</sup>, Thomas Thum<sup>8,9</sup>, Stefanie Dimmeler<sup>10</sup>, Peter Cserjesi<sup>11</sup>, Thomas Eschenhagen<sup>12</sup>, Paula A. da Costa Martins<sup>1,14</sup> and Leon J. De Windt<sup>1,14</sup>

**Although aberrant reactivation of embryonic gene programs is intricately linked to pathological heart disease, the transcription factors driving these gene programs remain ill-defined. Here we report that increased calcineurin/Nfat signalling and decreased *miR-25* expression integrate to re-express the basic helix-loop-helix (bHLH) transcription factor dHAND (also known as Hand2) in the diseased human and mouse myocardium. In line, mutant mice overexpressing Hand2 in otherwise healthy heart muscle cells developed a phenotype of pathological hypertrophy. Conversely, conditional gene-targeted *Hand2* mice demonstrated a marked resistance to pressure-overload-induced hypertrophy, fibrosis, ventricular dysfunction and induction of a fetal gene program. Furthermore, *in vivo* inhibition of *miR-25* by a specific antagomir evoked spontaneous cardiac dysfunction and sensitized the murine myocardium to heart failure in a Hand2-dependent manner. Our results reveal that signalling cascades integrate with microRNAs to induce the expression of the bHLH transcription factor Hand2 in the postnatal mammalian myocardium with impact on embryonic gene programs in heart failure.**

Growth of the heart during embryogenesis occurs primarily through proliferation of cardiac myocytes. Soon after birth, cardiac myocytes withdraw irreversibly from the cell cycle and subsequent growth of the heart occurs through hypertrophy rather than myocyte hyperplasia<sup>1–5</sup>. Cardiac hypertrophy entails an increase in muscle cell size secondary to increased mechanical load, as occurs in hypertension or valvular disease; to decreased mechanical performance, as occurs in ischaemic damage or intrinsic cardiac muscle disorders; or to neurohumoral stimulation as commonly occurs in cardiac dysfunction. It is also triggered in hereditary cardiomyopathies with seemingly normal performance and load<sup>6</sup>. Cardiac muscle characteristics in all of these settings include increased myocyte size, sarcomere formation and reprogramming of cardiac gene expression<sup>2,3,7,8</sup>. In humans, cardiac hypertrophy is

the principal risk factor for the development of heart failure and lethal arrhythmias<sup>6,9</sup>.

An intricate web of interconnected signalling modules has been implicated in hypertrophy of postnatal cardiomyocytes<sup>8</sup>, and these often culminate in the nucleus with activation of a defined set of transcription factors, some of which have prior roles in early heart development<sup>7</sup>. When activated in the adult myocardium, these signalling cascades reawaken a ‘fetal’ cardiac gene program<sup>1,8</sup>. Although elements of this program might be initial salutary adaptations to stress, it has become increasingly clear that the aberrant expression of fetal proteins involved in contractility, calcium handling and myocardial energetics leads to maladaptive changes in cardiac function<sup>1,3,10</sup>. Despite overwhelming evidence for the reactivation of ‘fetal’ gene programs

<sup>1</sup>Department of Cardiology, CARIM School for Cardiovascular Diseases, Maastricht University, 6229 ER Maastricht, The Netherlands. <sup>2</sup>Centre d'Etude de la Sensori-motricité, UMR 8194 CNRS, Université Paris Descartes, 75006 Paris, France. <sup>3</sup>Interuniversity Cardiology Institute Netherlands, Royal Netherlands Academy of Sciences, 3511 GC Utrecht, The Netherlands. <sup>4</sup>Department of Circulation and Medical Imaging, Norwegian University of Science and Technology (NTNU), NO-7491 Trondheim, Norway. <sup>5</sup>Department of Medical Physiology, University Medical Center Utrecht, 3584 CX Utrecht, The Netherlands. <sup>6</sup>Department of Pathology, University Medical Center Utrecht, 3584 CX Utrecht, The Netherlands. <sup>7</sup>Texas Heart Institute, Houston, Texas 77030, USA. <sup>8</sup>Institute of Molecular and Translational Therapeutic Strategies, Hannover Medical School, D-30625 Hannover, Germany. <sup>9</sup>National Heart and Lung Institute, Imperial College London, London SW7 2AZ, UK. <sup>10</sup>Institute of Cardiovascular Regeneration, Centre for Molecular Medicine, Goethe University, D-60590 Frankfurt am Main, Germany. <sup>11</sup>Department of Pathology and Cell Biology, Columbia University, New York 10032, USA. <sup>12</sup>Department of Experimental Pharmacology and Toxicology, University Medical Center Hamburg-Eppendorf, D-20246 Hamburg, Germany. <sup>13</sup>These authors contributed equally to this work.

<sup>14</sup>Correspondence should be addressed to P.A.d.C.M or L.J.D.W. (e-mail: [p.dacostamartins@maastrichtuniversity.nl](mailto:p.dacostamartins@maastrichtuniversity.nl) or [l.dewindt@maastrichtuniversity.nl](mailto:l.dewindt@maastrichtuniversity.nl))

in cardiac hypertrophy, canonical cardiogenic transcription factors, such as Nkx2-5 and Gata4 (refs 11–13), as the effectors of such a response, do not produce a classical hypertrophic response when reactivated in the adult myocardium. Conversely, there is strong evidence that transcriptional regulators including Camta2 (ref. 14), Nfat (refs 15,16), NF- $\kappa$ B (refs 17,18), Smads (refs 19,20) and Egr1 (refs 21,22) influence the cardiac hypertrophy response, but these factors probably do not participate in cardiogenesis. Thus, transcription factors that participate in both embryonic heart development and postnatal myocardial hypertrophy remain elusive, but the identification of such factors would facilitate the mechanistic link of ‘fetal’ gene reactivation to cardiac disease.

Transcription factors sharing a bHLH domain serve as key regulators of determination and differentiation of diverse cell types including skeletal muscle cells, haematopoietic cells and neuronal cells, and participate in mammalian cardiogenesis. The bHLH transcription factors heart and neural crest derivatives expressed transcript 2 (Hand2) and Hand1 are closely related members of the bHLH subclass of transcription factors required for proper heart development in the chick and mouse<sup>23–25</sup>. Hand2 is expressed in the second heart field and cardiac neural crest and deletion of Hand2 has shown that it is essential for right ventricle development and embryo survival beyond 10.5 days postconception<sup>23,26</sup>. In mice, Hand2 expression becomes specifically enhanced in the right ventricle after cardiac looping, whereas mouse Hand1 is expressed in left ventricular precursors<sup>27,28</sup>. Targeted deletion of *Hand2* in the neural crest lineage results in the misalignment of the outflow tract and aortic arch arteries<sup>29</sup>, similar to those observed in human congenital heart defects associated with neural crest defects<sup>30,31</sup>, providing strong evidence that Hand2 activity regulates development of the second heart field-derived myocardium.

## RESULTS

### Reactivating Hand2 causes cardiac dilation

Using two mouse models of heart failure and gene array analysis, we identified increased abundance of transcripts for *Hand2* in the failing heart (Fig. 1a). Western blot analysis confirmed upregulation of Hand2 protein in hearts from calcineurin transgenic mice (MHC–CnA; ref. 16) and in transverse aortic constriction (TAC) pressure-overloaded hearts<sup>15,32</sup>, two well-established animal models of maladaptive hypertrophy (Fig. 1b,c). Likewise, Hand2 protein and *Hand2* transcripts are elevated in biopsies of human cardiac tissue samples from heart failure patients when compared with human control heart tissue (Fig. 1d–f). To begin to address the functional role of Hand2 in postnatal cardiomyocyte function, we induced Hand2 expression in primary neonatal rat cardiomyocytes by infection with an adenovirus expressing full-length human Hand2 (Fig. 1g–i). To monitor changes in cell size or sarcomere organization, cardiomyocytes were stained for sarcomeric  $\alpha$ -actinin (Fig. 1h). Infection with AdHand2 resulted in a robust hypertrophic response as shown by a significant increase in cell size and in atrial natriuretic factor (ANF) expression (Fig. 1h,i), suggesting that Hand2 induction is sufficient to provoke a full hypertrophic response of cardiomyocytes *in vitro*. Furthermore, combinatorial stimulation with AdHand2 produces a more substantiated hypertrophic effect in cardiomyocytes secondary to stimulation with Nfat or Mef2a than with either factor alone, but not with Gata4 (Supplementary Fig. 1a,b).

To further understand the function of Hand2 induction in cardiac disease, we generated transgenic mouse lines overexpressing Hand2 in the postnatal myocardium using the alpha-myosin heavy chain (MHC) promoter<sup>33</sup>. Three transgenic lines were obtained each with different overexpression levels of Hand2 (Fig. 1j,k). All lines developed a cardiac phenotype, the severity of disease penetrance depending on the level of Hand2 overexpression (Fig. 1j–l). Line 2 Hand2 overexpressors with twofold overexpression of Hand2 developed a mild cardiac phenotype at 2 months of age, while Line 3 and 4 Hand2 overexpressors with three or sixfold overexpression of Hand2 developed signs of cardiac dilation (Fig. 1l). Specifically, Line 3 MHC–Hand2 mice exhibited wall thinning, myocyte disarray and hypertrophy (Fig. 1l and Supplementary Table 1). In addition, non-invasive analysis of cardiac function by serial Doppler echocardiography at 1 and 2 months of age revealed that Hand2 overexpression first provoked systolic and diastolic contractile defects (Fig. 1m–p) and progressively developed left ventricular dilatation (Fig. 1q), consistent with aspects of human heart failure. Quantification further indicated a reduction in left ventricular mass due to progressive wall thinning, hypertrophic myocytes (Fig. 1r,s and Supplementary Table 1) and re-expression of ‘fetal’ cardiac genes encoding the natriuretic peptides atrial natriuretic factor (*Nppa*), brain natriuretic peptide (*Nppb*) and  $\beta$ -myosin heavy chain (*Myh7*; Fig. 1t). Taken together, the data indicate that increased Hand2 expression is sufficient to provoke cardiomyocyte hypertrophy and cardiac dilation and dysfunction in the postnatal myocardium *in vivo*.

### Hand2 reactivation is required for heart disease

To begin to address the overall requirement of Hand2 in cardiac remodelling, we first tested different short hairpin RNAs (siRNAs) to provoke targeted knockdown of endogenous Hand2 by RNA-mediated interference (RNAi) *in vitro* (Fig. 2a,b). Next, cardiomyocytes were pretreated with scrambled siRNA or siRNA against Hand2 (Fig. 2c). Infection with AdCnA (ref. 34) or treatment with the prohypertrophic  $\alpha$ 1-adrenergic agonist phenylephrine after scrambled siRNA transfection resulted in a robust hypertrophic response as shown by a significant increase in cell size (Fig. 2c,d). RNAi against Hand2 abrogated the classical hypertrophic phenotype induced by AdCnA infection or phenylephrine treatment (Fig. 2c,d), suggesting that Hand2 is required to provoke a full hypertrophic response of cardiomyocytes *in vitro*.

Next, to assess the overall requirement of Hand2 in experimental heart failure in the mouse and to bypass the early embryonic lethality of *Hand2*-null mice<sup>23,29</sup>, we provoked deletion of a floxed *Hand2* (*Hand2*<sup>F/F</sup>) allele using a tamoxifen-inducible Cre recombinase protein fused to two mutant oestrogen-receptor ligand-binding domains<sup>35</sup> under control of the cardiac-specific  $\alpha$ -myosin heavy chain promoter (MHC–MCM mice; Fig. 2e). We optimized tamoxifen vehicle and dosing on the basis of previous reports to avoid transient toxicity effects<sup>36,37</sup> (Supplementary Fig. 2a–e). Subsequently, tamoxifen treatment of 8-week-old MCM–*Hand2*<sup>F/F</sup> mice induced efficient loss of *Hand2* transcripts and Hand2 protein in the heart as confirmed by quantitative real-time PCR and western blotting on heart tissue (Fig. 2f–h). We then tested the requirement of Hand2 in the development of cardiac disease in TAC pressure-overloaded hearts. To this end, *Hand2*<sup>F/F</sup> and MCM–*Hand2*<sup>F/F</sup> mice were treated with tamoxifen or vehicle for five consecutive days, and two days

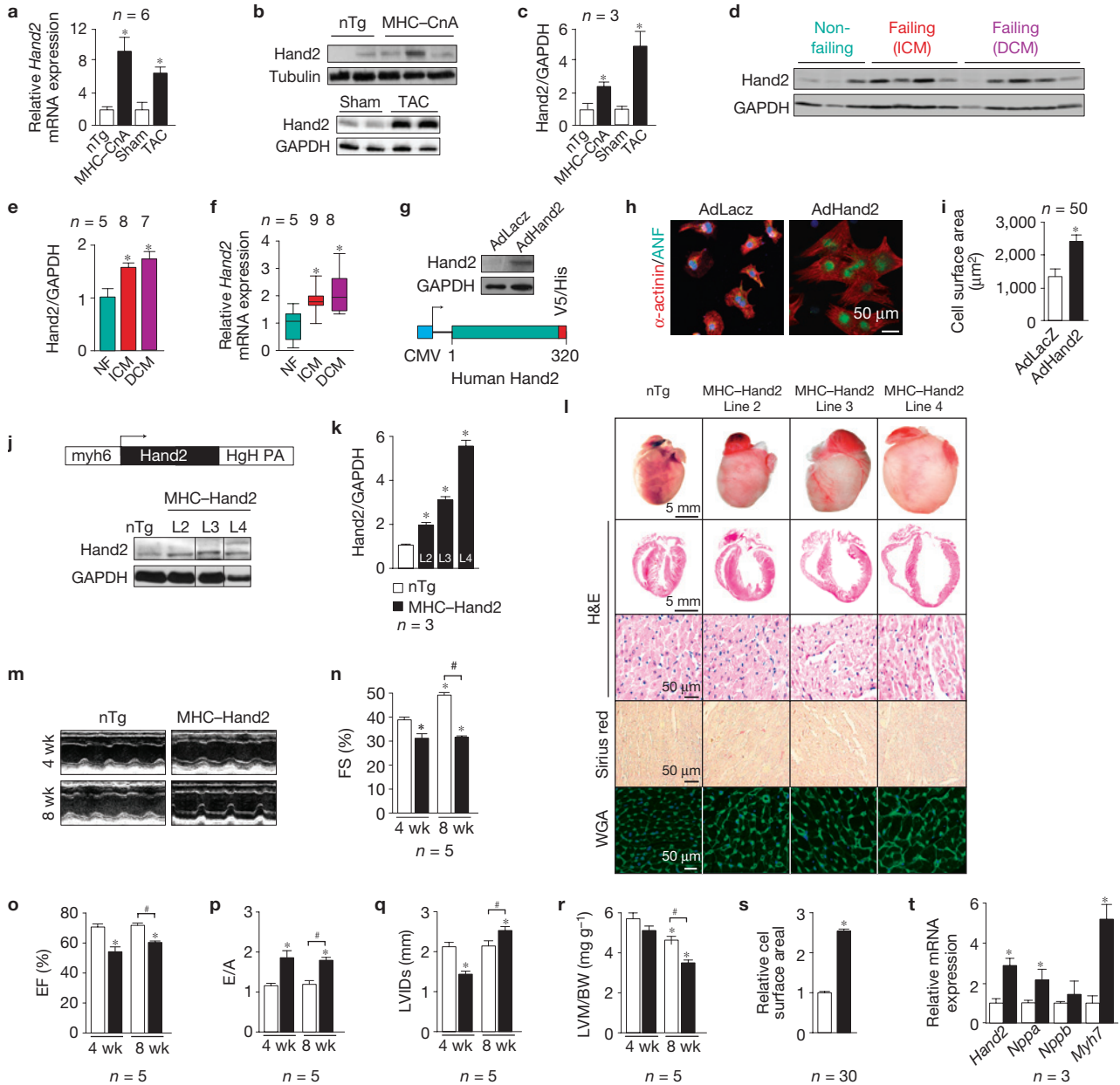


**Figure 1** Hand2 is reactivated in heart failure and sufficient to drive cardiac remodelling. **(a)** Quantitative real-time PCR analysis of *Hand2* transcript abundance in hearts from calcineurin transgenic mice (MHC-CnA) and mice subjected to TAC; *n*, number of hearts. **(b)** Western blot analysis of endogenous *Hand2*, tubulin or GAPDH as a loading control in hearts from non-transgenic (nTg) versus MHC-CnA and sham versus TAC mice. **(c)** Quantification of GAPDH-corrected *Hand2* western blot signals from **b**; *n*, number of hearts. **(d)** Representative images of western blot analysis of *Hand2* and GAPDH in human non-failing or failing myocardium. Failing human myocardium constituted ischaemic cardiomyopathy (ICM) or non-ischaemic dilated cardiomyopathy (DCM). **(e)** Quantification of GAPDH-corrected *Hand2* western blot signals from **d**; *n*, number of hearts. **(f)** Box plot quantitative representation of *HAND2* transcript abundance in human non-failing or failing myocardium (ICM or DCM); *n*, number of hearts. **(g)** Western blot of *Hand2* and GAPDH and schematic representation of Ad*Hand2* construct. **(h)** Confocal microscopy images of neonatal rat cardiomyocytes infected with AdLacZ or Ad*Hand2*; nuclei visualized with DAPI and stained with antibodies against  $\alpha$ -actinin (red) and ANF (green). **(i)** Quantification of cell surface area in conditions

in **h**; *n*, number of microscopic fields. **(j,k)** Design of transgenic vector (**j**, upper panel), western blot of *Hand2* and GAPDH (**j**, lower panel) and quantification (**k**); *n*, number of hearts. Lanes were spliced and samples were obtained and processed simultaneously. **(l)** Representative images of whole hearts (top panels), haematoxylin & eosin (H&E)-stained sections of four-chamber view (second panel), high-magnification sections (third panel), Sirius-red-stained sections (fourth panel) and wheat germ agglutinin (WGA)-stained (fifth panel) histological sections. **(m)** Representative M-mode images. **(n-r)** Quantification of fractional shortening (FS; **n**), ejection fraction (EF; **o**), E/A ratio (**p**), left ventricular internal diameter in systole (LVIDs; **q**) and left ventricular mass (LVM)/body weight (BW) ratio (**r**) of non-transgenic and MCM-*Hand2* L3 transgenic mice at 4 and 8 weeks of age; *n*, number of animals. **(s)** Quantification of cell surface areas in **i**; *n*, number of microscopic fields. **(t)** Quantitative real-time PCR analysis of *Hand2*, *Nppa*, *Nppb* and *Myh7*; *n*, number of hearts. \**P* < 0.05 versus corresponding control group; #*P* < 0.05 versus corresponding age group (error bars are s.e.m.). Black and white colour key for **n-t** is the same as in **k**. Source data are shown in Supplementary Table 9. Uncropped images of blots are shown in Supplementary Fig. 7.

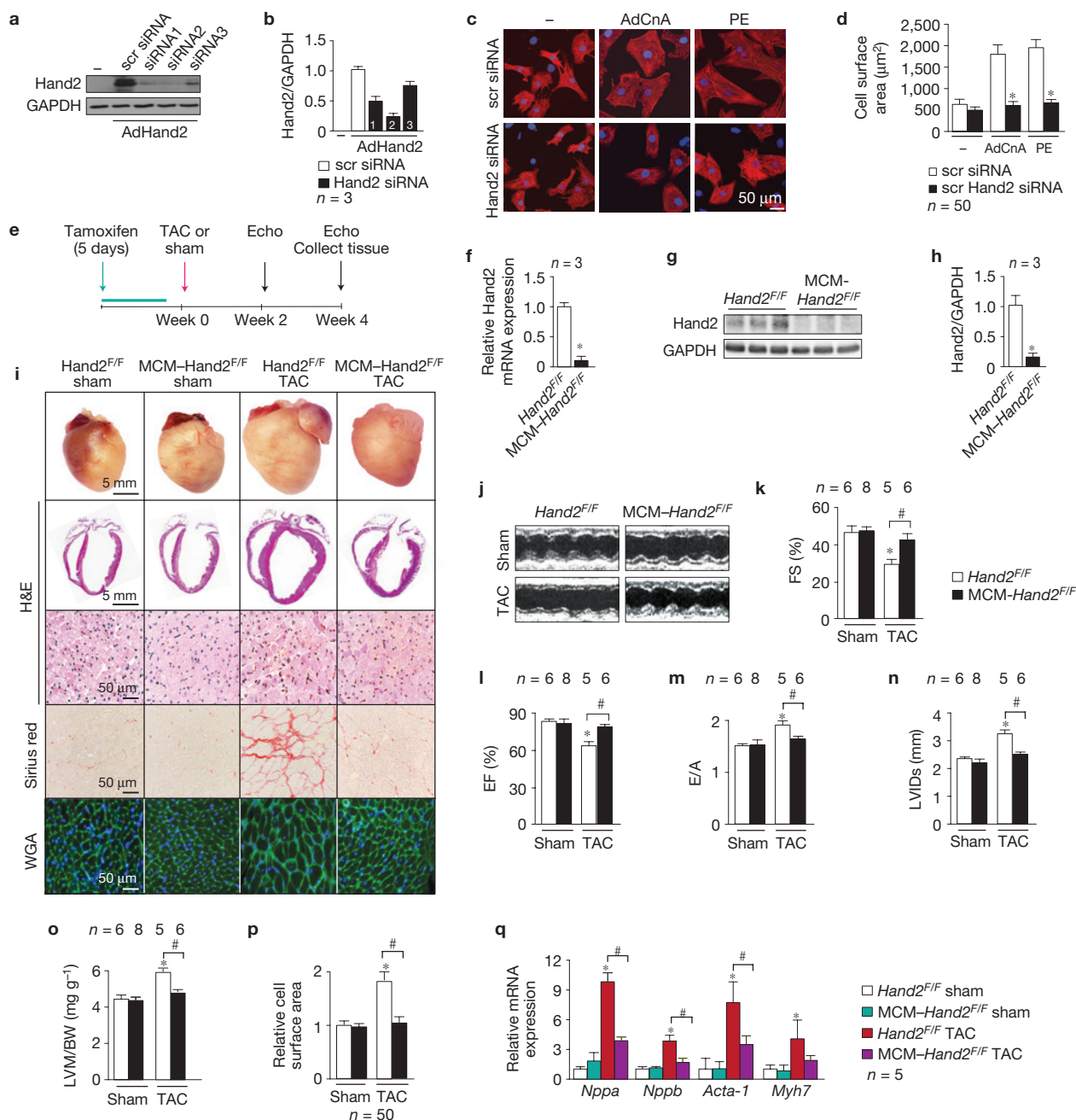
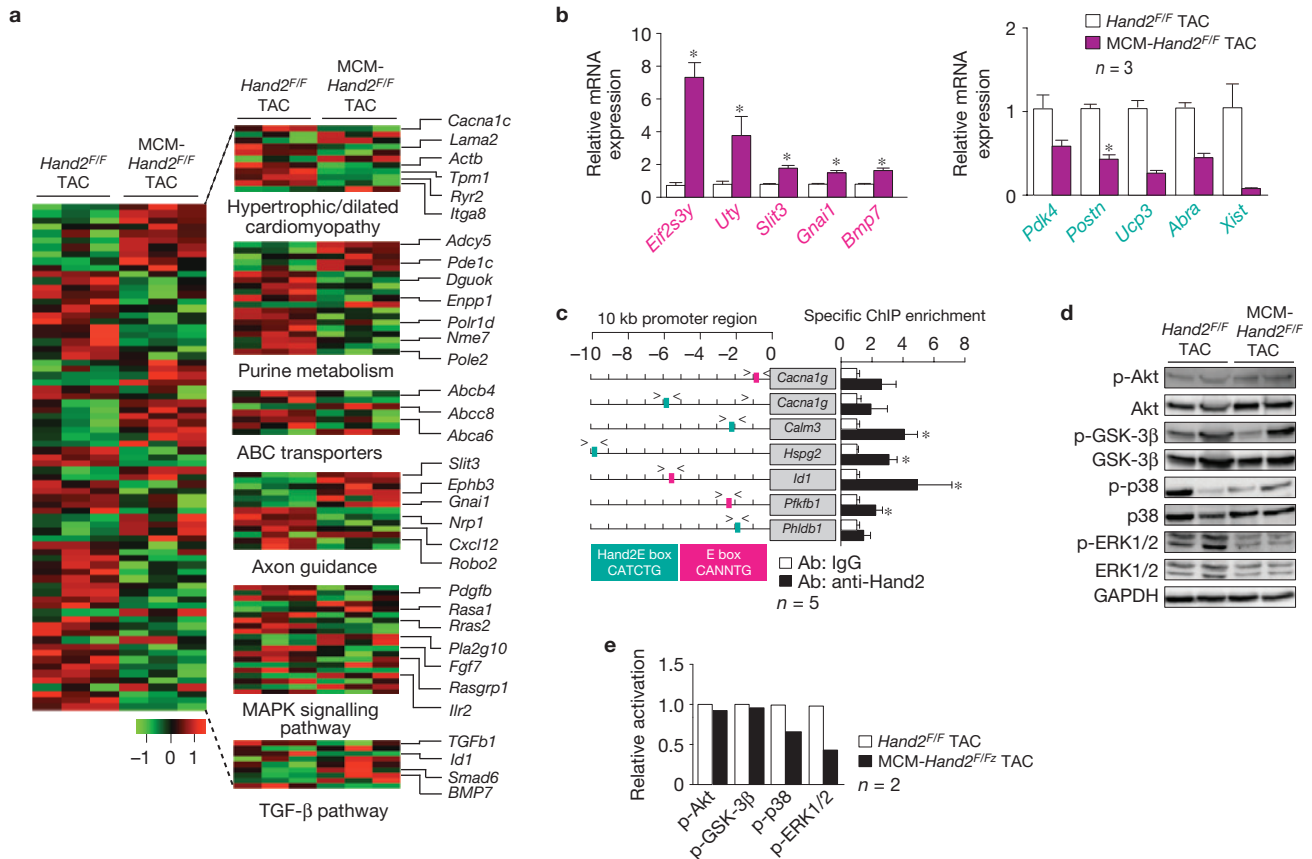


**Figure 2** Conditional Hand2 gene targeting. (a) Western blot analysis of Hand2 and GAPDH in cardiomyocytes without (–) or with AdHand2 infection and/or a scrambled siRNA and different siRNAs against Hand2. In AdHand2-infected cardiomyocytes, a scrambled siRNA and three different siRNAs against Hand2 (all predicted to target both rat and human Hand2) were tested for their strength to silence exogenous Hand2. (b) Western blot quantification; *n*, number of cell extracts. (c) Confocal microscopy images of neonatal rat cardiomyocytes in a control condition (–) or infected with AdCnA or treated with phenylephrine (PE) and transfected with scrambled siRNA or siRNA #2 against Hand2 from a, b. (d) Quantification of cell surface area in conditions in c; *n*, number of microscopic fields. (e) Design of the study. Adult Hand2<sup>F/F</sup> and MCM-Hand2<sup>F/F</sup> mice were treated with vehicle or tamoxifen for 5 days. TAC or sham surgery was performed 1 week after the first tamoxifen injection. Cardiac geometry and function were determined by serial Doppler echocardiography at 2 weeks and 4 weeks after surgery. (f) Quantitative real-time PCR analysis of Hand2; *n*, number of hearts. (g) Hand2 western blots in hearts from Hand2<sup>F/F</sup> and MCM-Hand2<sup>F/F</sup> mice after tamoxifen treatment.

(h) Western blot quantification; *n*, number of hearts. (i) Representative images of whole hearts (top panel), four-chamber view (second panel), H&E-stained sections (third panel), Sirius-red-stained sections (fourth panel) or WGA-stained (fifth panel) histological sections of hearts from tamoxifen-treated Hand2<sup>F/F</sup> and MCM-Hand2<sup>F/F</sup> mice subjected to sham or TAC surgery. (j) Representative M-mode images. (k–o) Quantification of fractional shortening (FS; k), ejection fraction (EF; l), E/A ratio (m), left ventricular internal diameter in systole (LVIDs; n) and left ventricular mass (LVM)/body weight (BW) ratio (o) of tamoxifen-treated Hand2<sup>F/F</sup> and MCM-Hand2<sup>F/F</sup> mice 4 weeks after sham or TAC surgery; *n*, number of animals. (p) Quantification of cell surface area from conditions in i; *n*, number of microscopic fields. Black and white colour key for l–p is the same as in k. (q) Quantitative real-time PCR analysis of *Nppa*, *Nppb*, *Acta-1* and *Myh7* in hearts from tamoxifen-treated Hand2<sup>F/F</sup> and MCM-Hand2<sup>F/F</sup> mice after sham or TAC surgery; *n*, number of hearts. \**P* < 0.05 versus corresponding control group; #*P* < 0.05 versus experimental group (error bars are s.e.m.). Source data are shown in Supplementary Table 9. Uncropped images of blots are shown in Supplementary Fig. 7.



later subjected to TAC pressure overload for four weeks (Fig. 2e). Cardiac size, myocyte disarray, interstitial and replacement fibrosis and cardiomyocyte size were significantly increased four weeks after TAC in *Hand2*<sup>F/F</sup> control mice, but *Hand2*-deficiency attenuated all these parameters of histopathological remodelling (Fig. 2i). Furthermore, non-invasive analysis of cardiac function by Doppler echocardiography demonstrated that targeted deletion of *Hand2* normalized fractional shortening and ejection fraction, and diastolic contractile defects, and attenuated left ventricular dilation compared with corresponding *Hand2*<sup>F/F</sup> or MHC-MCM control groups (Fig. 2j–n and Supplementary Tables 2 and 3). Post-mortem quantification further indicated that *Hand2* deficiency reduced left ventricular mass and myocyte cell size (Fig. 2o,p) and attenuated re-expression of ‘fetal’ cardiac genes *Nppa*, *Nppb*, *Acta1* and *Myh7*, but not splice isoform 4 of the gene encoding regulator of calcineurin 1 (*Rcan1-4*; Fig. 2q and Supplementary Fig. 2f).

Cardiac *Hand2* gene profiling  
Gene profiling of pressure-overloaded *Hand2*<sup>F/F</sup> and MCM-*Hand2*<sup>F/F</sup> mice revealed differentially expressed transcripts of cardiac Hand2 target genes (Fig. 3a and Supplementary Tables 4 and 5), which were validated by quantitative real-time PCR (Fig. 3b and Supplementary Fig. 3a,b). Notably, among the genes affected by Hand2 in the adult heart *in vivo*, we found several that have not previously been associated with the cardiac hypertrophic response (*Slit3*, *Ephb3*, *Robo2*, *Gnai1*, *Fgf7*), as well as a variety of candidate genes in the TGF $\beta$  pathway known to participate in cardiac hypertrophy (*Smad6*, *Bmp7*, *Tgfb1*; Fig. 3a; ref. 38). Interestingly, *Slit3*, *Ephb3*, *Robo2*, *Fgf7*, *Pdgfb* and *Lama2* have defined functions in embryonic heart development<sup>39–41</sup>, further lending evidence to the notion that Hand2 and its target genes are redeployed in the diseased postnatal myocardium. Bioinformatics analysis showed multiple (Hand2-specific) E-box binding sites<sup>42</sup> in

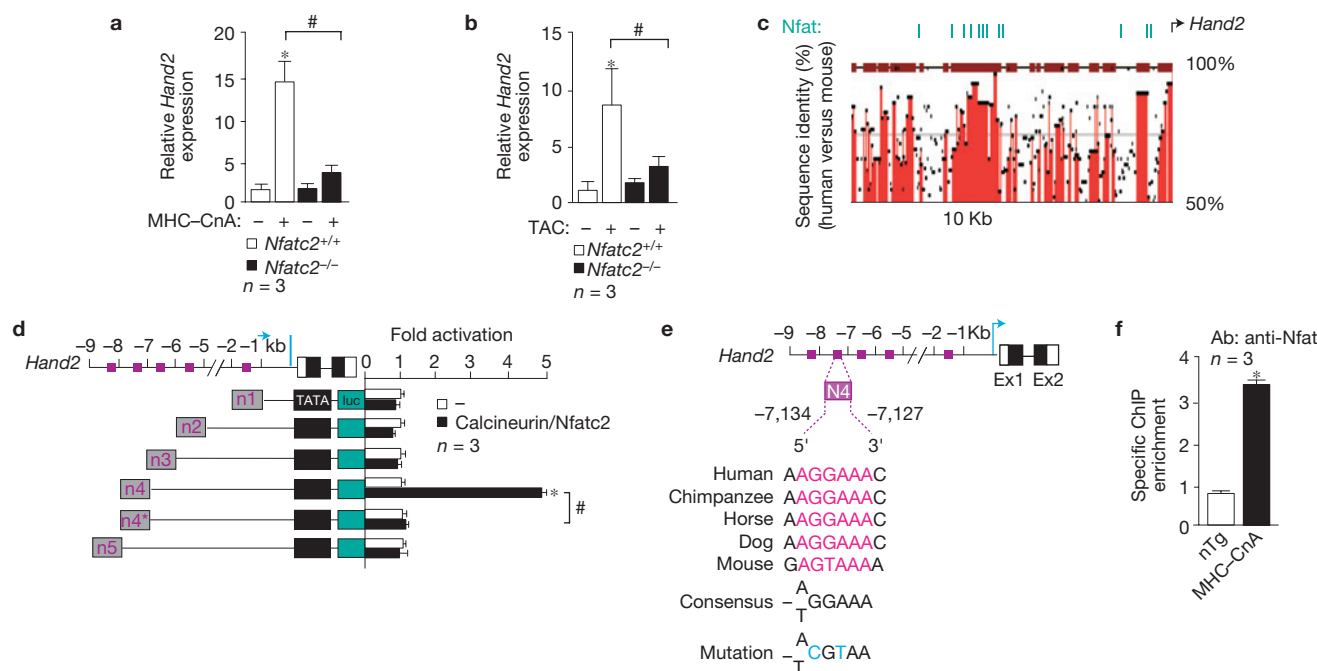


**Figure 4** Transcriptional regulation of cardiac *Hand2*. (a) Quantitative real-time PCR analysis of *Hand2* transcript abundance in hearts from calcineurin transgenic mice (MHC-CnA) crossbred with *Nfatc2*-null mice (*Nfatc2*<sup>-/-</sup>); *n*, number of hearts. (b) Quantitative real-time PCR analysis of *Hand2* transcript abundance in hearts from wild-type (*Nfatc2*<sup>+/+</sup>) and *Nfatc2*-null (*Nfatc2*<sup>-/-</sup>) mice subjected to TAC; *n*, number of hearts. (c) Comparison of the *Hand2* genomic regions between mouse and human as conservation percentage of a 10.0 kb genomic region upstream of the *Hand2* gene. (d) Luciferase reporter assays of 1–10 kb upstream genomic regions of the murine *Hand2* gene were tested for calcineurin/Nfat

responsiveness in transient transfection experiments in HEK293 cells. Luciferase reporters included a site-directed mutant for the N4 Nfat site located at  $-7.1$  kb; *n*, number of transfection experiments. (e) Schematic representation of the Nfat-binding site N4 showing its relative location to the murine *Hand2* start site and evolutionary conservation. (f) *In vivo* ChIP assay demonstrates that endogenous Nfatc2 is enriched on the Nfat-binding motif N4 in the *Hand2* gene in calcineurin transgenic hearts; nTg, non-transgenic; *n*, number of hearts. \* $P < 0.05$  versus control group; # $P < 0.05$  versus experimental group (error bars are s.e.m.). Source data are shown in Supplementary Table 9.

10-kilobase (kb) upstream promoter regions of *Hand2*-regulated genes, many of which could be further validated by chromatin immunoprecipitation (ChIP) with an antibody specific to *Hand2* (Fig. 3c). Finally, gene ontology analyses predicted that *Hand2* influences MAPK activation after biomechanical stress. Accordingly, the activation state of Akt, GSK-3 $\beta$  and terminal MAPK branches were investigated using phosphorylation-specific antibodies. No difference in activation of Akt or GSK-3 $\beta$  was found, but *Hand2* influenced p38 and ERK1/2 phosphorylation status (Fig. 3d,e). Taken together, *Hand2* deficiency provides protection against maladaptive cardiac remodelling and dysfunction following biomechanical stress in the adult heart and gene arrays identified a variety of target genes that are known to participate in cardiac hypertrophy but also uncovered *Hand2* target genes that have not yet been associated with cardiac remodelling.

### Transcriptional regulation of *Hand2*

In the developing embryo, transcriptional activation of the *Hand2* gene is governed by Gata4 activity and a cardiac enhancer located between  $-2.7$  and  $-4.2$  kb upstream of exon 1 (ref. 43). In addition, the *miR-1* genes (*miR-1-1* and *miR-1-2*) control *Hand2* protein expression and the balance between differentiation and proliferation during cardiogenesis<sup>44</sup>, indicating that *Hand2* protein levels in the embryo are titrated by integration of transcriptional and post-transcriptional mechanisms. In the postnatal myocardium, we found that *Hand2* was a direct target gene of the calcineurin/Nfat pathway *in vivo*, because

hearts from mice harbouring a null allele for *Nfatc2* exhibited less *Hand2* transcript induction following chronic activation of calcineurin signalling or pressure overload (Fig. 4a,b). A 10 kb region upstream of *Hand2* was scanned for evolutionarily conserved *cis* elements representing potential Nfat-binding sites (Fig. 4c). Luciferase activity experiments with deletion mutants and site-directed mutagenesis of the N4 Nfat consensus binding site revealed the existence of one evolutionarily conserved and functional Nfat site centred around  $-7.1$  kb upstream of the *Hand2* gene (Fig. 4d,e). Finally, the functionality of the N4 Nfat site was further demonstrated by *in vivo* ChIP with an Nfat antibody, further providing a mechanistic basis for the observed calcineurin/Nfat responsiveness of *Hand2* in the postnatal myocardium (Fig. 4f).

### Post-transcriptional regulation of *Hand2*

Apart from transcriptional activation, it is becoming increasingly clear that gene expression is also regulated at the post-transcriptional level by classes of non-coding RNAs. Following bioinformatics screens for microRNA binding sites in the 3'UTR of the *Hand2* gene and microRNA expression patterns that demonstrated an inverse expression in experimental models of heart disease, we identified *miR-1*, *miR-92a*, *miR-92b* and *miR-25* as possible candidates participating in post-transcriptional derepression of *Hand2* (Fig. 5a and Supplementary Fig. 4a; ref. 35). Most of these candidates belong to the miR-17 family that consists of three paralogous polycistronic clusters on different

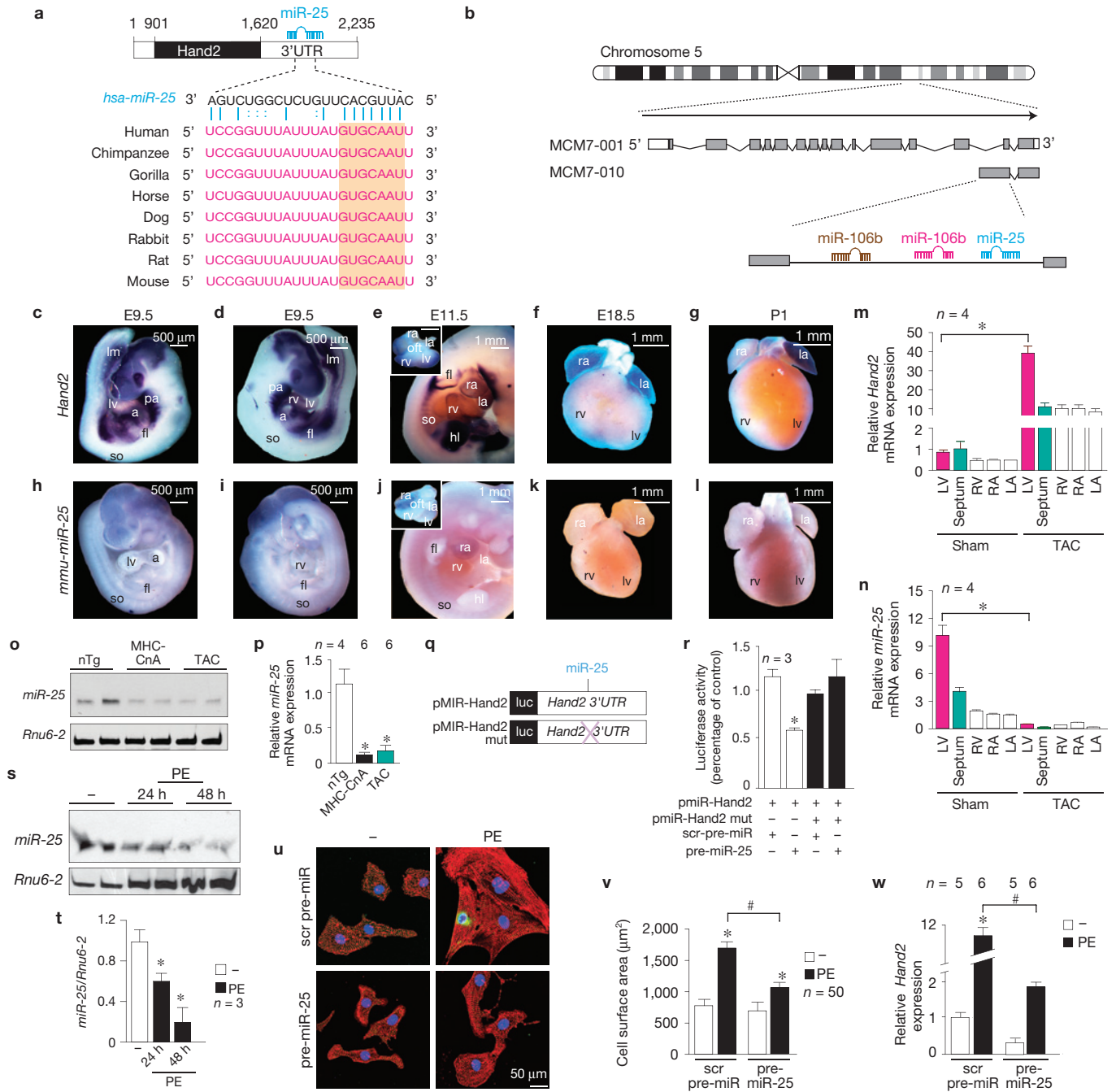


**Figure 5** Post-transcriptional regulation of Hand2 expression. **(a)** Location and evolutionary conservation of *hsa-miR-25* seed region on Hand2. **(b)** Schematic representation of two alternative *Mcm7* splice transcripts. **(c–g)** Representative images of whole-mount ISH for *Hand2* of E9.5 mouse embryos **(c,d)** and E11.5. Inset scale bar, 1 mm **(e)**. **(f,g)** Whole-mount ISH for *Hand2* in E18.5 heart **(f)** and heart 1 day after birth (P1) **(g)**. **(h–l)** Whole-mount ISH for *mmu-miR-25* of E9.5 **(h,i)** and E11.5 **(j)** mouse embryos. Inset scale bar, 1 mm **(j)**. **(k,l)** Whole-mount ISH for *mmu-miR-25* in E18.5 heart **(k)** and heart 1 day after birth (P1) **(l)**. a, atria; fl, forelimb; hl, hindlimb; lm, limb bud; la, left atrium; lv, left ventricle; of, outflow tract; pa, pharyngeal arches; ra, right atrium; rv, right ventricle; so, somites. **(m,n)** Quantitative real-time PCR analysis of *Hand2* **(m)** or *miR-25* **(n)** in left ventricular free wall (LV), intraventricular septum, right ventricular free wall (RV), right atrium (RA) and left atrium (LA) isolated from the adult murine heart subjected to 4 weeks of sham surgery or an adult heart subjected to 4 weeks of TAC surgery;  $n$ , number

of hearts. **(o)** Northern blot analysis of *miR-25* expression in hearts from non-transgenic (nTg) littermates, calcineurin transgenic mice (MHC-CnA) and mice subjected to TAC. *Rnu6-2* was used as a loading control. **(p)** Quantitative real-time PCR analysis of *miR-25* expression in hearts from non-transgenic littermates, calcineurin transgenic mice (MHC-CnA) and mice subjected to TAC;  $n$ , number of hearts. **(q)** Schematic representation of luciferase reporters. **(r)** Activity assay of luciferase reporter constructs in neonatal rat cardiomyocytes;  $n$ , number of transfection experiments. **(s)** Northern blot analysis of *miR-25*; *Rnu6-2* was used as a loading control. **(t)** Quantification of *miR-25* expression;  $n$ , number of cell extracts. PE, phenylephrine. **(u)** Confocal microscopy images. **(v)** Quantification of cell surface areas;  $n$ , number of microscopic fields. **(w)** Quantitative real-time PCR analysis of *Hand2*;  $n$ , number of culture dishes. \* $P < 0.05$  versus control group; # $P < 0.05$  versus experimental group (error bars are s.e.m.). Source data are shown in Supplementary Table 9. Uncropped images of blots are shown in Supplementary Fig. 7.

chromosomes: *miR-17 ~ 92* (*miR-17*, *miR-18a*, *miR-19a*, *miR-20a*, *miR-19b-1* and *miR-92a-1*), *miR-106b ~ 25* (*miR-106b*, *miR-93* and *miR-25*) and *miR-106a ~ 363* (*miR-106a*, *miR-18b*, *miR-20b*, *miR-19b-2*, *miR-92a-2* and *miR-363*). Members of each cluster belong to one of four groups with similar seed sequences and may share messenger RNA targets<sup>45</sup>. In line, *miR-1*, *miR-92a* and *miR-92b* exhibited reduced cardiac expression by northern blotting in mouse models of heart failure (Supplementary Fig. 4b–d), but specific silencing of *miR-92a* using an antagomir failed to influence cardiac *Hand2* transcript abundance or *Hand2* protein levels (Supplementary Fig. 4e–h).

*miR-25* is part of the intronic *miR-106b ~ 25* microRNA cluster in the minichromosome maintenance deficient 7 (*Mcm7*) gene (Fig. 5b). The mature form of *miR-25* is highly conserved from amphibians to primates (Supplementary Fig. 4i), and the *Hand2* 3'UTR harbours an evolutionarily conserved 7-seed region to *miR-25* (Fig. 5a). During cardiogenesis, *Hand2* is expressed in the cardiac crescent throughout cardiac specification<sup>27,28</sup>, downregulated in the future left ventricle and maintained along the outer curvature of the right ventricle and outflow tract<sup>28</sup>. This chamber-specification seems essential for morphogenesis as mice homozygous null for *Hand2* succumb at embryonic day (E)10.0 owing to failure to form a right ventricle and severe abnormalities in the neural crest-derived aortic arch arteries<sup>26,33</sup>. We detected *Hand2* in pharyngeal arches, future right ventricle, limb buds and craniofacial structures at E9.5 (Fig. 5c,d). At E11.5, expression in cardiogenic regions and the typical chamber-specific expression of *Hand2* became less pronounced (Fig. 5e). Before birth (E18.5), hearts exhibited only very weak *Hand2* expression in the ventricles and more pronounced expression in both atria (Fig. 5f). One day after birth, *Hand2* expression was virtually absent in ventricles and was further limited to expression in the left atrium (Fig. 5g). Whole-mount *in situ* hybridization (ISH) for *miR-25* demonstrated an absence of expression at E9.5 except for faint staining in craniofacial structures (Fig. 5h,i). At E11.5, *miR-25* was only transiently detectable in the future right atrium (Fig. 5j) and disappeared from the heart at E18.5 and shortly after birth (Fig. 5k,l). In line, endogenous *miR-25* was also expressed at a very low level in the fetal human heart compared with the adult, human non-failing myocardium (Supplementary Fig. 4j). To analyse whether *Hand2* and *miR-25* exhibit chamber-specific expression in the (diseased) adult myocardium, their expression was interrogated in separate cardiac compartments of sham- and TAC-operated mouse hearts. In the adult heart, *Hand2* is primarily expressed in the left ventricular free wall and septum and to a lesser extent in the right ventricle and atria. Following TAC, *Hand2* mRNA is increased in all cardiac compartments with the highest fold induction in the left ventricular free wall. In contrast, the induction of *Hand2* in the left ventricle and septum was accompanied by a strong repression of *miR-25* in the left ventricle and septum, indicating that *miR-25* repression may facilitate *Hand2* derepression in the adult left ventricle and septum (Fig. 5m,n). Northern blot profiling of *miR-25* indicated that this miR is not cardiac specific, although highly enriched in heart, lung and spleen (Supplementary Fig. 4k), and its expression is downregulated in the failing myocardium of established mouse models of heart failure (Fig. 5o,p). The dynamic cardiac expression pattern of *miR-25* in the healthy adult myocardium and failing heart is opposite to *Hand2* expression patterns and lends further credence for *miR-25*-based regulation of *Hand2* in the adult heart.

To more directly establish the regulation of *Hand2* by *miR-25* in the postnatal myocardium, we manipulated *miR-25* expression in cultured cardiomyocytes and in mouse hearts *in vivo*. Transient transfection of synthetic precursor *miR-25* in cardiomyocytes decreased *Hand2* 3'UTR reporter activity in a more pronounced manner than co-transfection with *miR-1*, *miR-92a* or *miR-92b* precursor molecules (Fig. 5q,r and Supplementary Fig. 4l). Primary cardiomyocytes stimulated with the prohypertrophic agonist phenylephrine also showed a downregulation of endogenous *miR-25* (Fig. 5s,t). *Hand2* transcript induction and hypertrophic cardiomyocyte remodelling after phenylephrine treatment was abrogated by transfection of *miR-25* precursor molecules (Fig. 5u–w), while pretreatment with antimir-25 provoked spontaneous hypertrophic growth even in the absence of stimuli (Supplementary Fig. 4m). In contrast, modulation of endogenous *miR-92a* or *miR-92b* did not influence cardiomyocyte hypertrophy *in vitro* to the same extent (Supplementary Fig. 5a,b). *miR-25* derepression and Nfat transcriptional activation act as two individual events controlling *Hand2* expression as evidenced by separate inhibition of either signalling event (Supplementary Fig. 5c,d). Moreover, cardiomyocyte hypertrophy induced by increased *Hand2* protein expression with a form of *Hand2* lacking the 3'UTR (Ad*Hand2*) was insensitive to *miR-25* levels (Supplementary Fig. 5c,d).

To evaluate whether the *miR-106b ~ 25* cluster is under the control of calcineurin/Nfat signalling, the expression levels of the primary and precursor forms of all cluster members were determined in hearts from mouse models of heart failure. In hearts from biomechanically stressed hearts, the expression of cluster members was not consistently downregulated. In contrast, in hearts from calcineurin transgenic mice all cluster members were very consistently and prominently downregulated (Supplementary Fig. 5e,f). In addition, two alternatively spliced *Mcm7* mRNAs that could give rise to the *miR-106b ~ 25* cluster were also significantly downregulated in calcineurin transgenic hearts (Supplementary Fig. 5g). Finally, specific inhibition of Nfat signalling with adenoviral VIVIT peptide<sup>46</sup> transduction derepressed *miR-25* and the two alternatively spliced *Mcm7* mRNA species in cultured cardiomyocytes (Supplementary Fig. 5h,i). Taken together, these data provide evidence for *miR-25*-based regulation of *Hand2* in the adult heart and that the downregulation of the *miR-106b ~ 25* cluster in the adult heart involves Nfat-dependent transcriptional repression.

### *miR-25* silencing exacerbates cardiac remodelling

Next, we made use of an antagomir to specifically silence endogenous *miR-25* expression *in vivo*. To this end, we designed chemically modified antisense oligonucleotides to target *Caenorhabditis elegans miR-39* as a control antagomir (ctrl antagomir) or *mmu-miR-25* (antagomir-25). Antagomirs were delivered by intraperitoneal injection on three consecutive days to wild-type mice randomized to receive sham or TAC surgery for four weeks (Fig. 6a) to test the ability of antagomir-25 to influence the development of postnatal cardiac disease. Cardiac *miR-25* expression was efficiently and specifically silenced (Fig. 6b and Supplementary Fig. 6a–c). Remarkably, antagomir-25 treatment sufficed to provoke signs of mild cardiac disease already in sham-operated mice as evidenced by increased cardiac size, mild fibrosis and myocyte size at four weeks after sham operation (Fig. 6c).

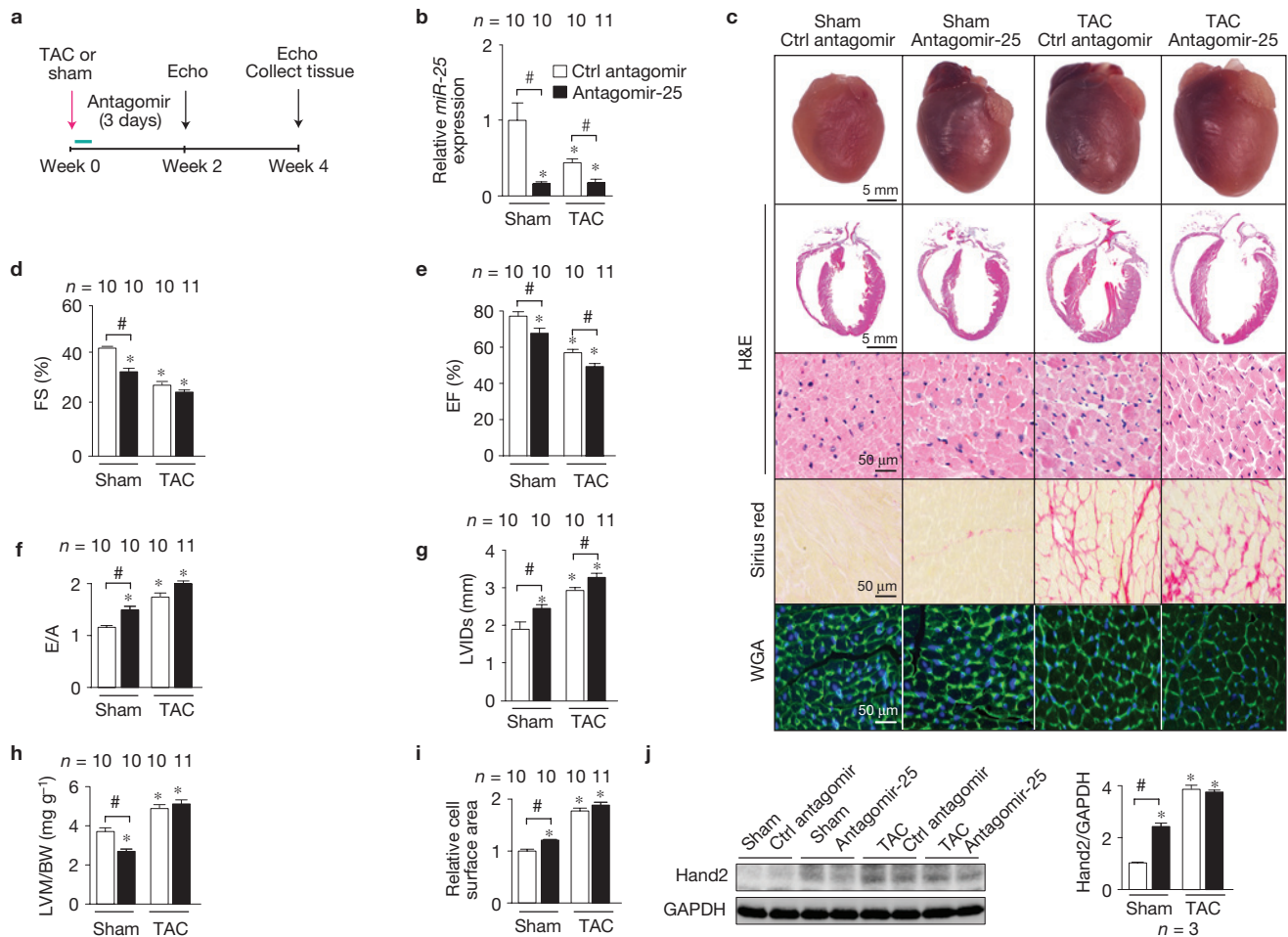


**Figure 6** *miR-25* silencing exacerbates cardiac remodelling. (a) Design of the study. Two-month-old mice were injected with control (ctrl) antagomir or antagomir against *miR-25* and subjected to sham or TAC surgery. Cardiac geometry and function was determined by serial Doppler echocardiography at 2 weeks and 4 weeks after surgery. (b) Quantitative real-time PCR analysis of *miR-25* expression in hearts from mice receiving control (ctrl) antagomir or antagomir against *miR-25* and subjected to sham or TAC surgery; *n*, number of hearts. (c) Representative images of whole hearts (top panels), haematoxylin & eosin (H&E)-stained sections of four-chamber view (second panel), high-magnification H&E-stained sections (third panel), Sirius-red-stained sections (fourth panel) and wheat germ agglutinin (WGA)-stained (fifth panel) histological sections. (d) Quantification of fractional shortening (FS). (e) Ejection fraction (EF). (f) E/A ratio obtained from pulsed-wave Doppler imaging of blood flow

Analysis of cardiac function by Doppler echocardiography also revealed that antagomir-25 treatment induced mildly reduced systolic and diastolic contractile function (Fig. 6d–f), provoked left ventricle (LV) dilation and increased heart weight (Fig. 6g,h). As expected, four weeks of TAC surgery in mice treated with a control antagomir provoked a substantial increase in myocyte disarray, interstitial fibrosis, cardiomyocyte size, systolic and diastolic dysfunction, left ventricular dilation, and increased heart weight, as well as an induction of the ‘fetal’ stress markers (Supplementary Fig. 6d). Strikingly, cardiac histopathology, cardiomyocyte hypertrophy, contractile function, the extent of left ventricular dilation and ventricular Hand2 protein levels were exacerbated by TAC surgery and antagomir-25 treatment (Fig. 6c–j and Supplementary Table 6). Taken together, these data

through the mitral valve during early (E) versus late (A) diastole. (g,h) Quantification of left ventricular internal diameter in systole (LVIDs; g) and the left ventricular mass (LVM)/body weight (BW) ratio (h) of mice treated with ctrl antagomir or antagomir-25 following sham or TAC surgery; *n*, number of animals. (i) Quantification of cell surface area of cardiomyocytes from mice treated with ctrl antagomir or antagomir-25 following sham or TAC surgery from conditions in c; *n*, number of microscopic fields. (j) Western blot for endogenous Hand2 in hearts from control antagomir- or antagomir-25-treated mice subjected to sham or TAC surgery and quantification of GAPDH-corrected Hand2 western blot signals; *n*, number of hearts. \**P* < 0.05 versus control group; #*P* < 0.05 versus experimental group (error bars are s.e.m.). Black and white colour key for d–j is the same as in b. Source data are shown in Supplementary Table 9. Uncropped images of blots are shown in Supplementary Fig. 7.

demonstrate that antagomir-mediated *miR-25* silencing evoked mild cardiac disease in sham-operated mouse hearts and exacerbated pressure-overload-induced cardiac remodelling.

### *miR-25* silencing fails to induce remodelling in Hand2 knockout hearts

Finally, to more directly establish the requirement of Hand2 in provoking spontaneous cardiac disease following *miR-25* silencing, 8-week-old MCM–*Hand2*<sup>FF</sup> mice were treated with vehicle or tamoxifen to provoke *Hand2* gene deletion for five consecutive days, and 2 days later treated with antagomir-25 or vehicle (Fig. 7a). Non-invasive analysis of cardiac geometry and function by Doppler echocardiography demonstrated that contractile function,

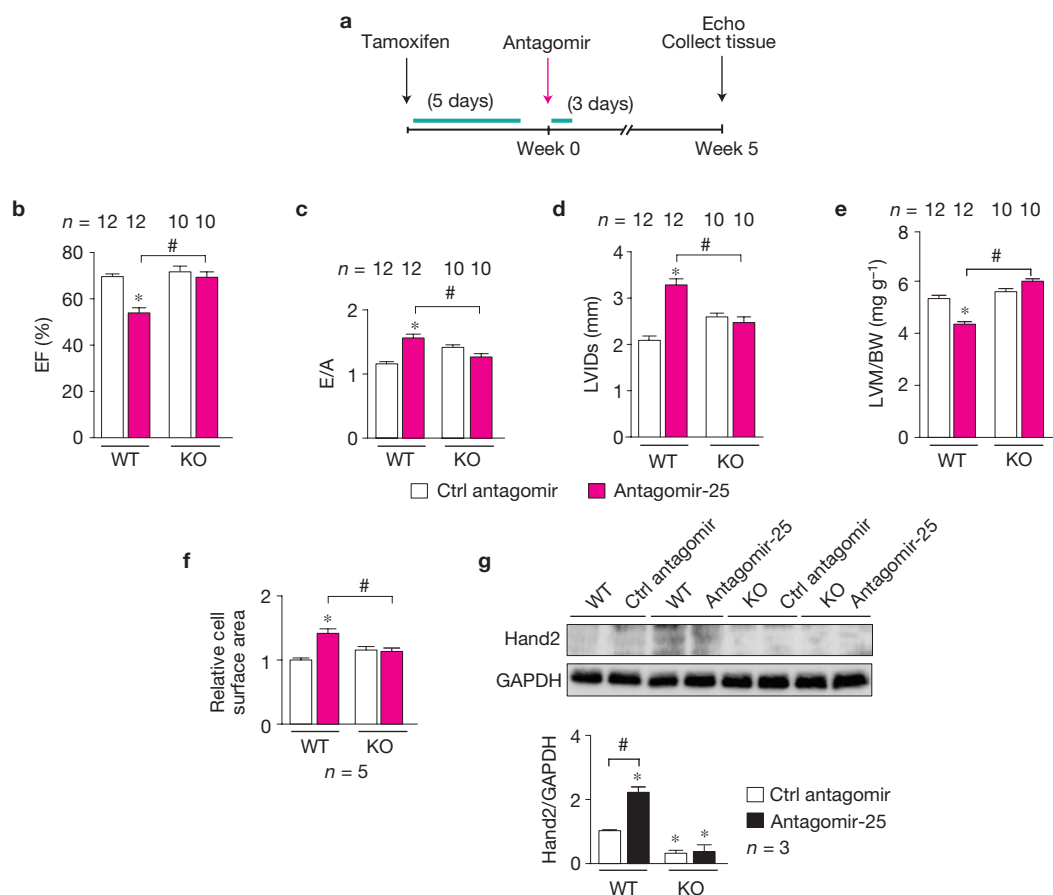


**Figure 7** *miR-25* silencing exacerbates cardiac remodelling. (a) Design of the study. MCM-*Hand2*<sup>F/F</sup> mice were injected with vehicle or tamoxifen for 5 consecutive days. One week after the first tamoxifen injection, mice received ctrl antagomir or antagomir-25 for 3 consecutive days. (b) Quantification of ejection fraction (EF). (c) E/A ratio from pulsed-wave Doppler imaging of blood flow through the mitral valve during early (E) versus late (A) diastole. (d,e) Left ventricular internal diameter in systole (LVIDs; d) and left ventricular mass (LVM)/body weight (BW) ratio (e) of MCM-*Hand2*<sup>F/F</sup> mice injected with PBS (WT) or tamoxifen (KO) and receiving ctrl antagomir or antagomir-25 for 4 weeks; *n*, number

of animals. (f) Quantification of cell surface areas of cardiomyocytes from MCM-*Hand2*<sup>F/F</sup> mice injected with PBS (WT) or tamoxifen (KO) and receiving ctrl antagomir or antagomir-25 for 4 weeks; *n*, number of hearts. (g) Western blot for Hand2 in hearts from MCM-*Hand2*<sup>F/F</sup> mice injected with PBS (WT) or tamoxifen (KO) and receiving ctrl antagomir or antagomir-25 for 4 weeks and quantification of GAPDH-corrected Hand2 western blot signals; *n*, number of hearts. \**P* < 0.05 versus control group; #*P* < 0.05 versus experimental group (error bars are s.e.m.). Source data are shown in Supplementary Table 9. Uncropped images of blots are shown in Supplementary Fig. 7.

left ventricular cavity size, heart weight and cardiomyocyte size were significantly increased four weeks after antagomir-25 treatment in MCM-*Hand2*<sup>F/F</sup> control mice (Fig. 7b–e) in line with earlier observations (Fig. 6d–g). In contrast, *Hand2*-deficiency normalized systolic and diastolic contractile function (Fig. 7b,c), attenuated left ventricular dilatation (Fig. 7d), and normalized heart weight and cardiomyocyte hypertrophy (Fig. 7e,f) on antagomir-25 treatment (Supplementary Table 7). In line, ventricular Hand2 protein levels were derepressed by antagomir-25 treatment, but nearly absent in the *Hand2*-deficient heart (Fig. 7g). Combined, our data reveal that stress-induced Hand2 expression in the postnatal myocardium is regulated by a combinatorial interplay of calcineurin/Nfat transcriptional induction and post-transcriptional derepression by *miR-25* (Fig. 8).

## DISCUSSION

Many signalling modules implicated as necessary for hypertrophy of the postnatal myocardium engage cellular circuits that control

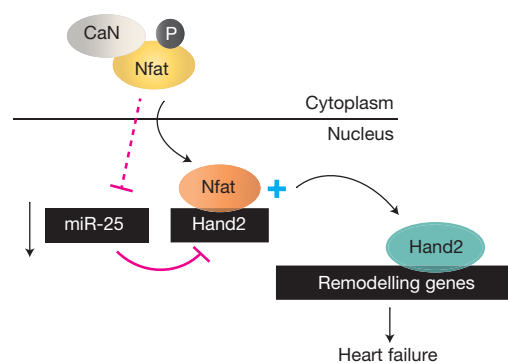


**Figure 8** Hand2 regulation in the postnatal myocardium by a combined calcineurin/Nfat transcriptional and *miR-25* post-transcriptional axis. Model depicting the activation of calcineurin/Nfat signalling under cardiac stress, resulting in Nfat-mediated transcriptional activation of the *Hand2* gene and Nfat-mediated transcriptional repression of *miR-25*, which cooperatively reactivates Hand2 to provoke expression of Hand2 target genes, cardiac remodelling and heart failure.

growth and gene expression in the embryonic heart. Here we report the discovery of a transcriptional regulator of postnatal gene expression and growth. Our data show for the first time that the bHLH transcription factor Hand2, required for proper heart development in the chick and mouse, is re-employed in the failing heart to drive the induction of a gene circuit that controls cardiac growth, dilation and dysfunction. Mechanistically, activation of the *Hand2* gene occurs by an enhancer sequence harbouring a phylogenetically conserved Nfat site centred around 7 kb upstream of the Hand2 start site. Equally important, a mechanism involving post-transcriptional derepression by *miR-25*, which is strongly repressed in human and mouse heart failure models, also controls the expression of Hand2. The finding that a microRNA-dependent mechanism is involved in Hand2 induction in the postnatal myocardium further identifies a possible additional site of therapeutic intervention for heart failure by the class of RNA therapeutics. Indeed, in the past years, examples of pathological heart failure mechanisms involving microRNAs that were repairable with RNA therapeutics now include pathological cardiac hypertrophy and signalling<sup>47–49</sup>, loss of contractility<sup>50</sup>, increased autophagy, apoptosis and ageing<sup>51,52</sup>, excessive fibrosis<sup>53</sup>, impaired angiogenesis<sup>54</sup> and deficits in heart muscle regeneration<sup>4</sup>. The re-expression of Hand2 in the postnatal myocardium is the first example in the field where classical signalling cascades are interconnected with microRNA-mediated derepression and cooperatively enforce an integrated response driving expression of a bHLH transcription factor in control of embryonic gene programs, cardiac growth and features of heart failure. □

## METHODS

Methods and any associated references are available in the [online version of the paper](#).

*Note: Supplementary Information is available in the online version of the paper*

## ACKNOWLEDGEMENTS

We gratefully acknowledge G. Summer for bioinformatics help and G. van Hout for technical support. T.T. was supported by the German Research Foundation (TH903/11-1) and the REBIRTH Excellence Cluster. T.E. was supported by the German Research Foundation (ES88/12-1) and the DZHK, the German Centre for Cardiovascular Research funded by the German Ministry of Research and Education (BMBF). P.A.d.C.M. was supported by a Leducq Career Development Award and the Dutch Heart Foundation grant NHS2010B261. L.J.D.W. acknowledges support from the Netherlands CardioVascular Research Initiative: the Dutch Heart Foundation, Dutch Federation of University Medical Centers, the Netherlands Organization for Health Research and Development (ZonMW) and the Royal Netherlands Academy of Sciences. L.J.D.W. was further supported by a VIDI award 917-863-72 from the ZonMW; the Dutch Heart Foundation program grant NHS2007B167; the Fondation Leducq Transatlantic Network of Excellence program 08-CVD-03 and grant 311549 from the European Research Council (ERC).

## AUTHOR CONTRIBUTIONS

E.D., P.A.d.C.M., M.M.G., L.E.P., K.S., M.B. and N.K. performed northern blots and quantitative real-time PCR experiments. M.M.G., S.O. and S.S. performed western blots. E.D. and M.M.G. performed luciferase assays. S.L. performed bioinformatics analyses. E.D., V.K. and S.O. performed chromatin immunoprecipitation assays. A.-S.A. and C.C. performed mouse embryo studies. Y.M., P.C., S.O. and L.J.D.W. created genetically modified mouse models. H.e.A. and N.B. performed surgical procedures in mouse models. E.D., P.A.d.C.M., M.M.G., R.N., K.S., N.B. and G.J.J.d.S. performed echocardiography and histology in mouse models. E.D., P.A.d.C.M., M.M.G., A.-S.A., K.S., S.L. and L.J.D.W. analysed data. C.C., S.H., P.G.A.V., T.T., S.D., P.C. and T.E. provided reagents, models or data. E.D., P.A.d.C.M. and L.J.D.W. designed the study. E.D., P.A.d.C.M. and L.J.D.W. wrote the manuscript. P.A.d.C.M. and L.J.D.W. acquired funding for the study. E.D. and M.M.G. contributed equally as joint first authors. P.A.d.C.M. and L.J.D.W. contributed equally as joint last authors.

## COMPETING FINANCIAL INTERESTS

The authors declare no competing financial interests.

Published online at [www.nature.com/doi/10.1038/ncb2866](http://www.nature.com/doi/10.1038/ncb2866)

Reprints and permissions information is available online at [www.nature.com/reprints](http://www.nature.com/reprints)

- Olson, E. N. & Schneider, M. D. Sizing up the heart: development redux in disease. *Genes Dev.* **17**, 1937–1956 (2003).
- Katz, A. M. The cardiomyopathy of overload: an unnatural growth response. *Eur. Heart J.* **16**, 110–114 (1995).
- Hoshijima, M. & Chien, K. R. Mixed signals in heart failure: cancer rules. *J. Clin. Invest.* **109**, 849–855 (2002).
- Eulalio, A. *et al.* Functional screening identifies miRNAs inducing cardiac regeneration. *Nature* **492**, 376–381 (2012).
- Senyo, S. E. *et al.* Mammalian heart renewal by pre-existing cardiomyocytes. *Nature* **493**, 433–436 (2013).
- Towbin, J. A. & Bowles, N. E. The failing heart. *Nature* **415**, 227–233 (2002).
- Oka, T., Xu, J. & Molkenin, J. D. Re-employment of developmental transcription factors in adult heart disease. *Semin. Cell Dev. Biol.* **18**, 117–131 (2007).
- Heineke, J. & Molkenin, J. D. Regulation of cardiac hypertrophy by intracellular signalling pathways. *Nat. Rev. Mol. Cell Biol.* **7**, 589–600 (2006).
- Savage, D. D., Levy, D., Dannenberg, A. L., Garrison, R. J. & Castelli, W. P. Association of echocardiographic left ventricular mass with body size, blood pressure and physical activity (the Framingham Study). *Am. J. Cardiol.* **65**, 371–376 (1990).
- Meijs, M. F. *et al.* Left ventricular hypertrophy: a shift in paradigm. *Curr. Med. Chem.* **14**, 157–171 (2007).
- Aries, A., Paradis, P., Lefebvre, C., Schwartz, R. J. & Nemer, M. Essential role of GATA-4 in cell survival and drug-induced cardiotoxicity. *Proc. Natl Acad. Sci. USA* **101**, 6975–6980 (2004).
- Oka, T. *et al.* Cardiac-specific deletion of Gata4 reveals its requirement for hypertrophy, compensation, and myocyte viability. *Circ. Res.* **98**, 837–845 (2006).
- Bar, H., Kreuzer, J., Cojoc, A. & Jahn, L. Upregulation of embryonic transcription factors in right ventricular hypertrophy. *Basic Res. Cardiol.* **98**, 285–294 (2003).
- Song, K. *et al.* The transcriptional coactivator CAMTA2 stimulates cardiac growth by opposing class II histone deacetylases. *Cell* **125**, 453–466 (2006).
- Bourajaj, M. *et al.* NFATc2 is a necessary mediator of calcineurin-dependent cardiac hypertrophy and heart failure. *J. Biol. Chem.* **283**, 22295–22303 (2008).
- Molkenin, J. D. *et al.* A calcineurin-dependent transcriptional pathway for cardiac hypertrophy. *Cell* **93**, 215–228 (1998).
- Freund, C. *et al.* Requirement of nuclear factor- $\kappa$ B in angiotensin II- and isoproterenol-induced cardiac hypertrophy *in vivo*. *Circulation* **111**, 2319–2325 (2005).
- Li, Y. *et al.* NF- $\kappa$ B activation is required for the development of cardiac hypertrophy *in vivo*. *Am. J. Physiol. Heart Circ. Physiol.* **287**, H1712–H1720 (2004).
- Wang, J. *et al.* Targeted disruption of Smad4 in cardiomyocytes results in cardiac hypertrophy and heart failure. *Circ. Res.* **97**, 821–828 (2005).
- Xu, J. *et al.* GDF15/MIC-1 functions as a protective and antihypertrophic factor released from the myocardium in association with SMAD protein activation. *Circ. Res.* **98**, 342–350 (2006).
- Buitrago, M. *et al.* The transcriptional repressor Nab1 is a specific regulator of pathological cardiac hypertrophy. *Nat. Med.* **11**, 837–844 (2005).
- Saadane, N., Alpert, L. & Chalifour, L. E. Altered molecular response to adrenoceptor-induced cardiac hypertrophy in Egr-1-deficient mice. *Am. J. Physiol. Heart Circ. Physiol.* **278**, H796–H805 (2000).
- Srivastava, D., Cserjesi, P. & Olson, E. N. A subclass of bHLH proteins required for cardiac morphogenesis. *Science* **270**, 1995–1999 (1995).
- Cross, J. C. *et al.* Hxt encodes a basic helix-loop-helix transcription factor that regulates trophoblast cell development. *Development* **121**, 2513–2523 (1995).
- Hollenberg, S. M., Sternglanz, R., Cheng, P. F. & Weintraub, H. Identification of a new family of tissue-specific basic helix-loop-helix proteins with a two-hybrid system. *Mol. Cell Biol.* **15**, 3813–3822 (1995).
- Srivastava, D. *et al.* Regulation of cardiac mesodermal and neural crest development by the bHLH transcription factor, dHAND. *Nature Genet.* **16**, 154–160 (1997).
- Biben, C. & Harvey, R. P. Homeodomain factor Nkx2-5 controls left/right asymmetric expression of bHLH gene eHand during murine heart development. *Genes Dev.* **11**, 1357–1369 (1997).
- Thomas, T., Yamagishi, H., Overbeek, P. A., Olson, E. N. & Srivastava, D. The bHLH factors, dHAND and eHAND, specify pulmonary and systemic cardiac ventricles independent of left-right sidedness. *Dev. Biol.* **196**, 228–236 (1998).
- Morikawa, Y. & Cserjesi, P. Cardiac neural crest expression of Hand2 regulates outflow and second heart field development. *Circ. Res.* **103**, 1422–1429 (2008).
- Snider, P., Olaopa, M., Firulli, A. B. & Conway, S. J. Cardiovascular development and the colonizing cardiac neural crest lineage. *Sci. World J.* **7**, 1090–1113 (2007).
- Hutson, M. R. & Kirby, M. L. Model systems for the study of heart development and disease. Cardiac neural crest and conotruncal malformations. *Semin. Cell Dev. Biol.* **18**, 101–110 (2007).
- Rockman, H. A. *et al.* Segregation of atrial-specific and inducible expression of an atrial natriuretic factor transgene in an *in vivo* murine model of cardiac hypertrophy. *Proc. Natl Acad. Sci. USA* **88**, 8277–8281 (1991).

33. Subramaniam, A. *et al.* Tissue-specific regulation of the alpha-myosin heavy chain gene promoter in transgenic mice. *J. Biol. Chem.* **266**, 24613–24620 (1991).
34. De Windt, L. J. *et al.* Calcineurin-mediated hypertrophy protects cardiomyocytes from apoptosis *in vitro* and *in vivo*: an apoptosis-independent model of dilated heart failure. *Circ. Res.* **86**, 255–263 (2000).
35. Zhang, Z. *et al.* The microRNA-processing enzyme Dicer is dispensable for somite segmentation but essential for limb bud positioning. *Dev. Biol.* **351**, 254–265 (2011).
36. Sohal, D. S. *et al.* Temporally regulated and tissue-specific gene manipulations in the adult and embryonic heart using a tamoxifen-inducible Cre protein. *Circ. Res.* **89**, 20–25 (2001).
37. Koitabashi, N. *et al.* Avoidance of transient cardiomyopathy in cardiomyocyte-targeted tamoxifen-induced MerCreMer gene deletion models. *Circ. Res.* **105**, 12–15 (2009).
38. Koitabashi, N. *et al.* Pivotal role of cardiomyocyte TGF-beta signaling in the murine pathological response to sustained pressure overload. *J. Clin. Invest.* **121**, 2301–2312 (2011).
39. Fish, J. E. *et al.* A Slit/miR-218/Robo regulatory loop is required during heart tube formation in zebrafish. *Development* **138**, 1409–1419 (2011).
40. Baker, R. K., Vanderboom, A. K., Bell, G. W. & Antin, P. B. Expression of the receptor tyrosine kinase gene EphB3 during early stages of chick embryo development. *Mech. Dev.* **104**, 129–132 (2001).
41. Mason, I. J., Fuller-Pace, F., Smith, R. & Dickson, C. FGF-7 (keratinocyte growth factor) expression during mouse development suggests roles in myogenesis, forebrain regionalisation and epithelial-mesenchymal interactions. *Mech. Dev.* **45**, 15–30 (1994).
42. Dai, Y. S. & Cserjesi, P. The basic helix-loop-helix factor, HAND2, functions as a transcriptional activator by binding to E-boxes as a heterodimer. *J. Biol. Chem.* **277**, 12604–12612 (2002).
43. McFadden, D. G. *et al.* A GATA-dependent right ventricular enhancer controls dHAND transcription in the developing heart. *Development* **127**, 5331–5341 (2000).
44. Zhao, Y., Samal, E. & Srivastava, D. Serum response factor regulates a muscle-specific microRNA that targets Hand2 during cardiogenesis. *Nature* **436**, 214–220 (2005).
45. Tanzer, A. & Stadler, P. F. Molecular evolution of a microRNA cluster. *J. Mol. Biol.* **339**, 327–335 (2004).
46. Aramburu, J. *et al.* Affinity-driven peptide selection of an NFAT inhibitor more selective than cyclosporin A. *Science* **285**, 2129–2133 (1999).
47. Care, A. *et al.* MicroRNA-133 controls cardiac hypertrophy. *Nat. Med.* **13**, 613–618 (2007).
48. da Costa Martins, P. A. *et al.* MicroRNA-199b targets the nuclear kinase Dyrk1a in an auto-amplification loop promoting calcineurin/NFAT signalling. *Nature Cell Biol.* **12**, 1220–1227 (2010).
49. Ganesan, J. *et al.* MiR-378 controls cardiac hypertrophy by combined repression of mitogen-activated protein kinase pathway factors. *Circulation* **127**, 2097–2106 (2013).
50. Van Rooij, E. *et al.* Control of stress-dependent cardiac growth and gene expression by a microRNA. *Science* **316**, 575–579 (2007).
51. Ucar, A. *et al.* The miRNA-212/132 family regulates both cardiac hypertrophy and cardiomyocyte autophagy. *Nat. Commun.* **3**, 1078 (2012).
52. Boon, R. A. *et al.* MicroRNA-34a regulates cardiac ageing and function. *Nature* **495**, 107–110 (2013).
53. Thum, T. *et al.* MicroRNA-21 contributes to myocardial disease by stimulating MAP kinase signalling in fibroblasts. *Nature* **456**, 980–984 (2008).
54. Bonauer, A. *et al.* MicroRNA-92a controls angiogenesis and functional recovery of ischemic tissues in mice. *Science* **324**, 1710–1713 (2009).

## METHODS

**Human heart samples.** Approval for studies on human tissue samples was obtained from the Medical Ethics Committee of the University Medical Center Utrecht, The Netherlands, and by the Ethical Committee of the University Hospital Hamburg, Germany (Az. 532/ 116/ 9.7.1991). All patients or their relatives gave written informed consent before operation. In this study, we included tissue from the left ventricular free wall of patients with end-stage heart failure secondary to ischaemic heart disease. Control tissue was taken from the left ventricular free wall of refused donor hearts. Failing hearts were also obtained from patients undergoing heart transplantation because of terminal heart failure. Non-failing donor hearts that could not be transplanted for technical reasons were used for comparison, where neither donor patient histories nor echocardiography revealed signs of heart disease.

**Mouse models.** A human full-length *Hand2* cDNA was cloned into the Sall/HindIII sites downstream of a 5.5 kb murine cardiac alpha-myosin heavy chain promoter (*Myh6*, U71441) construct (gift from J. Robbins, Cincinnati Children's Hospital Medical Center, Cincinnati, Ohio, USA) to generate the transgenic vector MHC-Hand2. Before oocyte injection, BamHI digestion removed the bacterial backbone of the vector before injection into the pronuclei of fertilized FVB/N oocytes, which were transferred to the oviducts of pseudopregnant FVB/N recipients. Transgenic founders and progeny were identified by PCR analysis of genomic DNA using primers directed against the polyA tail of the transgene, 5'-GTCTGACTAGGTGCTCTTCT-3', 5'-CGTCTCTCTGCTGGTATAG-3'. Both male and female MHC-Hand2 transgenic mice of 4 weeks and 8 weeks of age were used for functional and histological analysis. Mice harbouring a floxed allele of *Hand2* (*Hand2<sup>fl/fl</sup>*) in a B6129F1 background were described previously,<sup>55</sup> and crossed with mice harbouring a tamoxifen-regulated form of Cre recombinase (MerCreMer) under control of the murine *Myh6* promoter (MHC-MerCreMer; MCM mice)<sup>36</sup> in a B6129F1 background to generate MCM-*Hand2<sup>fl/fl</sup>* mice. *Hand2<sup>fl/fl</sup>* and MCM-*Hand2<sup>fl/fl</sup>* were treated with either vehicle (10/90 v/v ethanol/peanut oil, Sigma P2144) or tamoxifen (45 mg kg<sup>-1</sup> per day) by daily intraperitoneal injections for 5 consecutive days. Both male and female, adult MCM-*Hand2<sup>fl/fl</sup>* mice and *Hand2<sup>fl/fl</sup>* mice (8–10 weeks of age) were used for functional and histological analyses. Other mice used in this study were male calcineurin transgenic mice in a B6CBAF1/J background expressing an activated mutant of calcineurin in the postnatal heart under control of the 5.5 kb murine *Myh6* promoter (MHC-CnA; ref. 16), and male and female B6CBAF1/J wild-type mice (Charles River Laboratories) of 2–6 months of age. All animal studies were performed in accordance with local institutional guidelines and regulations. Sample size was determined by a power calculation based on an echocardiographic effect size. Randomization of subjects to experimental groups was based on a single sequence of random assignments. Animal caretakers blinded investigators to group allocation during the experiment and/or when assessing the outcome.

**Antagomir studies.** Chemically modified antisense oligonucleotides designed to target *C. elegans miR-39-5p* (5'-AAGGCAAGCUGACCCUGAAGUU-3'/3CholTEG-3') with a 3' cholesterol conjugation and 2 phosphorothioate bonds at the very first 5' end and 4 phosphorothioate bonds between the last 3' bases<sup>56</sup> that does not target mammalian sequences as control antagomir (ctrl antagomir) and an antagomir specific for *miR-25-3p* (5'-UCAGACCGAGACAAGUGCAAUG-3'/3CholTEG-3'; antagomir-25) were synthesized at Integrated DNA Technologies (IDT). Female and male B6CBAF1 mice (8–10 weeks of age) were subjected to sham or TAC surgery. Following 3 days, mice were injected (intraperitoneally) with antagomir-25 (80 mg kg<sup>-1</sup> body weight) or ctrl antagomir (80 mg kg<sup>-1</sup> body weight) for 3 consecutive days. Echo analysis was performed at 2 weeks and 4 weeks after surgery. Adult MCM-*Hand2<sup>fl/fl</sup>* mice (8–10 weeks of age) were treated with phosphate-buffered saline (PBS) or tamoxifen (dissolved in peanut oil) for 5 consecutive days (45 mg kg<sup>-1</sup>/day). Seven days after the last tamoxifen injection, mice were injected (intraperitoneally) with antagomir-25 (80 mg kg<sup>-1</sup> body weight) or vehicle (PBS) for three consecutive days.

**Aortic banding and transthoracic echocardiography.** Transverse aortic constriction (TAC) or sham surgery was performed in 2–3-month-old BL6CBAF1 mice by subjecting the aorta to a defined 27 gauge constriction between the first and second truncus of the aortic arch as described previously<sup>15,32</sup>. For Doppler echocardiography, mice were shaved and lightly anaesthetized with isoflurane (mean 3% in oxygen) and allowed to breathe spontaneously through a nasal cone. Non-invasive, echocardiographic parameters were measured using a RMV707B (15–45 MHz) scan-head interfaced with a Vevo-770 high-frequency ultrasound system (VisualSonics). Long-axis EKG-triggered cine loops of the left ventricular

(LV) contraction cycle were obtained in B-mode to assess end-diastolic/systolic volume. Short-axis recordings of the LV contraction cycle were taken in M-mode to assess wall thickness of the anterior/posterior wall at the mid-papillary level. Doppler was used to determine the ratio between early (E) and late (A) ventricular filling velocity (E/A ratio) and to calculate the pressure gradient between the proximal and distal sites of the TAC and only mice with a pressure gradient >50 mm Hg were included. From B-mode recordings, LV length from basis to apex, LV internal diameter in systole (LVIDs) and diastole (LVIDd) were determined. From M-mode recordings, LV posterior wall thickness in systole (LV PWs) and diastole (LV PWd) were determined. LV mass was calculated with the following formula:  $(0.8 \times (1.04 \times (((LVIDd + LV PWd + IVSd)^3) - ((LVIDd)^3)) + 0.6)$ ; fractional shortening (FS) was calculated with the following formula:  $(LVIDd - LVIDs)/LVIDd \times 100$ . Ejection fraction (EF) was calculated as  $((SV/Vd) \times 100)$  with Vs, systolic volume  $(3.1416 \times (LVIDs^3)/6)$ , Vd, diastolic volume  $(3.1416 \times (LVIDd^3)/6)$ , and SV, stroke volume  $(Vd - Vs)$ .

**Histological analysis and (immunofluorescence) microscopy.** Hearts were arrested in diastole, perfusion fixed with 4% paraformaldehyde/PBS solution, embedded in paraffin and sectioned at 4 μm. Paraffin sections were stained with haematoxylin and eosin for routine histological analysis; Sirius red for the detection of fibrillar collagen; and FITC-labelled wheat-germ-agglutinin (Sigma-Aldrich, 1:100) to visualize and quantify myocyte cross-sectional area. Slides were visualized using a Zeiss Axioskop 2Plus with an AxioCamHRc. Cell surface areas were determined using ImageJ imaging software (<http://rsb.info.nih.gov/ij/>).

**Chromatin immunoprecipitation.** For *in vivo* Nfat chromatin immunoprecipitation (ChIP), hearts from wild-type and MHC-CnA mice were perfusion-fixed with 1% paraformaldehyde/PBS solution. Ventricular tissue was dounce-homogenized and sonicated to obtain soluble chromatin. ChIP was carried out using the Upstate Biotechnology ChIP assay kit according to the manufacturer's instructions using rabbit polyclonal against h-Nfatp (ref. 57), provided by N.R. Rice (National Cancer Institute, Frederick Cancer Research and Development Center, USA). Equal amounts of soluble chromatin from each sample were immunoprecipitated with antisera. Following immunoprecipitation and immobilization of immunocomplexes, reverse crosslinking was achieved by incubation at 65 °C for 4 h. Associated DNA was purified by phenol/chloroform extraction and PCR was carried out using specific primers surrounding the Nfat motif using primers directed against the mouse *Hand2* gene (NM\_010402.4), 5'-AGCCTTGAGGTTGAAGGCTCTG-3', 5'-CAAAGCTGGTGGAAAGGCGA-3'. ChIP input was normalized using primers directed against the mouse myoglobin gene (NM\_01164047), 5'-GGAAGTCTCTACGGTCTGT-3', 5'-AGGTCCTCTGAGCCCTTCAT-3'. For *in vitro* Hand2 ChIP,  $3 \times 10^6$  neonatal rat ventricular cardiomyocytes were seeded in 10 cm dishes and infected for 24 h with AdGFP or AdHand2. Cells were crosslinked with 1% formaldehyde at room temperature and stopped after 10 min using 125 mM glycine. Nuclei were isolated from fixed cells with 5 mM PIPES at pH 8.0, 85 mM KCl and 0.5% NP-40 containing protease inhibitors. DNA was extracted from nuclei in 50 mM Tris at pH 8.1, 10 mM EDTA and 1% SDS, plus protease inhibitors for 10 min on ice and subsequently sonicated to fragments of 0.3–1.5 kb. After clearing debris, samples were diluted fivefold in 0.01% SDS, 1.1% Triton X-100, 1.2 mM EDTA, 16.7 mM Tris and 167 mM NaCl containing protease inhibitors and pre-cleared with 80 μl salmon sperm/protein A agarose slurry for 30 min at 4 °C on rotation. Beads were pelleted, supernatant divided and incubated with or without 5 μg of rabbit polyclonal anti-Hand2 (Santa Cruz, sc-22818). Immune complexes were collected with 60 μl of salmon sperm DNA/protein A agarose slurry for 1 h at 4 °C on rotation. Beads were subjected to the following washes at volumes of 1 ml low-salt: 0.1% SDS, 1% Triton X-100, 2 mM EDTA, 20 mM Tris at pH 8.1 and 150 mM NaCl, high-salt: 0.1% SDS, 1% Triton X-100, 2 mM EDTA, 20 mM Tris at pH 8.1 and 500 mM NaCl, twice in 1 × TE buffer. After washing, complexes were eluted in 250 μl of fresh 1% SDS and 0.1 M NaHCO<sub>3</sub> for 15 min on continuous vortex and cleared from beads. Crosslinkage was reverted by incubation with 10 μg RNase and NaCl to a final concentration of 0.3 M at 65 °C for 5 h followed by a classical ethanol-based DNA precipitation. Collected DNA was resuspended in 100 μl of double-distilled H<sub>2</sub>O supplemented with 2 μl of 0.5 M EDTA, 4 μl of 1 M Tris at pH 6.5 and 1 μl of 20 mg ml<sup>-1</sup> proteinase K for antibody digestion at 45 °C for 2 h. Finally, DNA was purified by application to QiaQuick spin columns (Qiagen GmbH) and PCR was carried out using specific primers for *Cacna1g*, *Calm3*, *Hspg2*, *Idl1*, *Pfkfb1* and *Phldb1*. Primer sequences are provided in Supplementary Table 8.

**In situ hybridization.** The Hand2 probe was provided by V. Christoffels (Academic Medical Center, Amsterdam, The Netherlands), linearized with EcoRI, re-

verse transcribed using T7 RNA polymerase and labelled with digoxigenin–ddUTP using the 3′-end-labelling kit (Roche). *Mmu-miR-25* was detected using the *miR-25* LNA probe from Exiqon. Procedures for *in situ* hybridization were performed as described previously<sup>58</sup> with some modifications. Embryos were fixed overnight at 4 °C in 4% paraformaldehyde/PBS, and then washed in PBS. Fresh embryos were treated for 15 min at room temperature with 10 µg ml<sup>-1</sup> proteinase K, washed for 5 min with 2 mg ml<sup>-1</sup> glycine in PBST (PBS containing 0.1% Tween-20), and then with PBS and further fixed in 4% paraformaldehyde/0.2% glutaraldehyde in PBS for 20 min. Embryos were transferred to the hybridization buffer (50% paraformamide, 5 × SSC, 2% blocking powder (Boehringer), 0.1% Tween-20, 0.5% CHAPS, 50 µg ml<sup>-1</sup> yeast transfer RNA, 5 mM EDTA and 50 µg ml<sup>-1</sup> heparin) and pre-hybridized for 1 h at 70 °C (for Hand2 detection) and at 55 °C (for miR-25 detection). Hybridizations were performed in fresh pre-heated hybridization buffer containing digoxigenin-labelled antisense probes as follows: 5 nM of labelled LNA probe (up to 5 days for miR-25) or 0.1 µg ml<sup>-1</sup> (overnight for Hand2). Post-hybridization washes were performed at the hybridization temperature by successive incubations for 10 min in hybridization buffer diluted in increasing concentration of 2 × SSC (25%, 50%, 75%), before washing twice for 10 min at room temperature and then twice for 30 min at 70 °C in 100 mM maleic buffer and 150 mM NaCl. Then embryos were washed in PBS and twice for 10 min in 2 mM levamisole TBST (0.14 M NaCl, 2.7 mM KCl, 25 mM Tris-HCl at pH 7.5 and 0.1% Tween-20). After 2–3 h blocking at room temperature in 10% sheep serum (diluted in 2 mM levamisole TBST), embryos were incubated overnight at 4 °C in 1% sheep serum/2 mM levamisole TBST using anti-digoxigenin mouse monoclonal HRP antibody (Lifespan Biosciences, LS-C64859-200 clone 21H8, 1:2,000). The next day, mouse embryos were washed 6 × 1 h and overnight in 2 mM levamisole TBST at room temperature. After the post-antibody washes, embryos were washed in 2 mM levamisole NTMT (100 mM NaCl, 100 mM Tris-HCl at pH 9.5, 50 mM MgCl<sub>2</sub> and 0.1% Tween-20). Staining was realized in NBT/BCIP (Roche) and diluted 50 × in NTMT. The reaction was stopped in 10 mM EDTA/PBST and embryos were 1 h fixed in 4% paraformaldehyde/0.2% glutaraldehyde in PBS. Embryos were then kept at 4 °C in 10 mM EDTA/PBST.

**Western blot analysis.** Whole tissue or cell lysates were produced in RIPA buffer supplemented with PhosSTOP (Roche) and Protease inhibitor cocktail (Roche). Subsequently samples were boiled in 4 × Laemmli buffer, including 2% β-mercaptoethanol, for 5 min at 95 °C. SDS-PAGE and western blotting were performed using the Mini-PROTEAN 3 system (Bio-Rad). Blotted membranes were blocked in 5% BSA/TBS-Tween. Primary antibody labelling was performed overnight at 4 °C. Secondary HRP-conjugated antibodies were applied for 1 h at room temperature. After each antibody incubation, blots were washed for 3 × 10 min in TBS-Tween. Images were generated using Supersignal West Dura Extended Duration ECL Substrate (Pierce) and the LAS-3000 documentation system (FujiFilm Life Science). Stripping was performed with Restore Western blot stripping buffer (Pierce). Outputs were normalized for loading. Antibodies used included mouse monoclonal anti-HAND2 (Sigma-Aldrich, 1105 clone 4H8, 1:500), rabbit polyclonal anti-HAND2 (Santa Cruz, sc-22818, 1:500), goat polyclonal monoclonal anti-V5 (Abcam, ab9137, 1:5,000), mouse monoclonal anti-GAPDH (Millipore, MAB374 clone 6C5, 1:10,000), rabbit polyclonal anti-α-tubulin (Cell Signaling Technology, #2144, 1:1,000), polyclonal rabbit anti-mouse IgG-horseradish-peroxidase (HRP; DAKO, P0161, 1:5,000), polyclonal swine anti-rabbit IgG-HRP (DAKO, P0399, 1:5,000), rabbit polyclonal phospho-p44/42 MAPK (Cell Signaling Technology, #9101, 1:1,000), rabbit polyclonal p44/42 MAPK (Cell Signaling Technology, #9102, 1:1,000), rabbit polyclonal phospho-AKT (Cell Signaling Technology, #9271, 1:1,000), rabbit polyclonal AKT (Cell Signaling Technology, #9172, 1:1,000), rabbit polyclonal phospho-p38 MAPK (Cell Signaling Technology, #9211, 1:1,000), mouse monoclonal p38 MAPK (BD, #61269, 1:1,000), rabbit polyclonal phospho-GSK-3β (Cell Signaling Technology, #9336, 1:1,000) and rabbit polyclonal GSK-3β (Cell Signaling Technology, 9315, 1:1,000).

**Northern blot analysis.** Northern blotting was performed as described previously<sup>48</sup> using 3′-digoxigenin-labelled locked nucleic acid oligonucleotides for *miR-25*, *miR-92a*, *miR-92b*, *miR-1* and U6 small nuclear RNA (*Rnu6-2*). Detection was achieved with Fab fragments from polyclonal anti-digoxigenin antibodies, conjugated to alkaline phosphatase (Roche, 11093274910, 1:5,000).

**Quantitative real-time PCR.** Total RNA (1 µg) was applied to either miR-based or mRNA-based reverse transcription. Quantitative real-time PCR was performed according to SYBRgreen methodology. Transcript quantities were normalized for endogenous loading. Primer sequences are provided in Supplementary Table 8.

**Primary cardiomyocytes cultures, immunocytochemistry and adenoviral infections.** Cardiomyocyte cultures were isolated by enzymatic dissociation of 1–2-day-old neonatal rat hearts and processed for immunofluorescence microscopy as described previously<sup>59</sup>. Neonatal cardiomyocytes were transfected with precursors (Ambion) and inhibitors (Exiqon) of microRNAs (10 mM) using Oligofectamine (Invitrogen). For visualization of cardiomyocyte size and sarcomeric organization, the cells were stained for α-actinin with mouse monoclonal anti-sarcomeric α-actinin antibody (Sigma-Aldrich, A7811 clone EA-53, 1:500) followed by rat anti-mouse phenylephrine-Texas red-conjugated monoclonal antibody (Life Technologies, RM2817 clone M1/70.15, 1:800). Perinuclear atrial natriuretic factor expression was visualized using a rabbit polyclonal anti-atrial natriuretic factor antibody (Bachem, T-4014, 1:800) followed by a secondary anti-rabbit Oregon green-conjugated antibody (Life Technologies, A-889, 1:1,000). Nuclear staining was performed with VECTASHIELD Mounting Medium (Vector Laboratories) with 4′,6-diamidino-2-phenylindole (DAPI). Myocyte hypertrophy was induced by infecting cells with AdCnA<sup>34</sup> or by stimulation for 24 h with phenylephrine (10 µM) as described earlier<sup>34</sup>. To generate AdHand2, the human Hand2 ORF sequence was PCR subcloned into pCDNA4/V5–His to generate a 3′ V5–His tag and subsequently PCR cloned into the pDC516 adenoviral shuttle vector, and subjected to FLP–frt homologous recombination to generate AdHand2. Other adenoviruses used include AdMEF2A (ref. 60), AdGATA4 (ref. 61), AdΔNfat (ref. 62), AdGFP (ref. 63), AdLacZ (ref. 34) and AdvVIT (ref. 63).

**Luciferase-reporter assays.** Neonatal rat cardiomyocytes were transfected with the 5 µg pMIR-report plasmid (Ambion) containing a fragment of 700 bp of the 3′UTR of mouse Hand2 (pMIR-Hand2) using Eugene 6 reagent (Roche), followed by transfection with 10 nM of *miR-25*, *miR-92a*, *miR-92b*, *miR-1* or scrambled miR precursor molecules using Oligofectamine (Invitrogen). Low-passage HEK293 cells were grown in DMEM (Invitrogen) supplemented with 10% FBS. HEK293 cells (2 × 10<sup>5</sup>) were seeded in 24-well plates and transfected at 50–60% confluency with a total of 2 µg DNA in DMEM containing 2% FBS with 1.5 µl FuGENE 6 reagent (Roche) per microgram of DNA. A series of mouse Hand2 promoter deletion fragments were generated by PCR as XhoI–HindIII fragments and subcloned into the pGL3 reporter plasmid (Promega). The integrity of all deletion constructs was confirmed by sequencing. For co-transfection assays, 0.3 µg per well of pGL3–Hand2 reporter construct was transfected with 0.3 µg per well of pCDNA3–ΔCnA and pEF–BOS–hNFATp (ref. 64), pRL–TK (Promega; 0.2 µg per well), containing the thymidine kinase promoter driving *Renilla* luciferase, was included to correct for transfection efficiency. The total amount of DNA per well was adjusted to 1.2 µg using pCDNA3 empty vector. The cells were washed 24 h after transfection with PBS and lysed with 100 µl of Reporter Lysis Buffer (Roche). Lysates were examined by application to the Dual Luciferase assay kit (Promega) on a 96-well Topcount liquid scintillation counter (Packard Instruments).

**Affymetrix gene array analyses.** Cardiac RNA was collected from ventricular tissue of 3 tamoxifen-injected *Hand2<sup>fl/fl</sup>* and 3 tamoxifen-injected *MCM–Hand2<sup>fl/fl</sup>* mice (4 weeks after sham or TAC surgery) and subjected to GeneChip Mouse Gene 1.0 ST Array (Affymetrix) according to the manufacturer’s recommendations. The assay started with 4–8 µg total RNA sample. The detection probes were made by *in situ* synthesis using photo-generated reagent chemistry. Hybridization used 100 µl × SSPE buffer (0.90 M NaCl, 60 mM Na<sub>2</sub>HPO<sub>4</sub> and 6 mM EDTA, at pH 6.8) containing 25% formamide at 34 °C. After RNA hybridization, tag-conjugating Cy3 or Cy5 dyes were circulated through the microfluidic chip for dye staining. Fluorescence images were collected using a laser scanner (GenePix 4000B, Molecular Devices) and digitized using Array-Pro image analysis software (Media Cybernetics). DAVID v 6.7. (The Database for Annotation, Visualization and Integrated Discovery.) <http://david.abcc.ncifcrf.gov/> was used as a tool to provide functional interpretation of genes obtained from microarray. Classification of the differentially expressed genes to specific signalling pathways was performed with the use of KEGG (Kyoto Encyclopedia of Genes and Genomes) database <http://www.genome.jp/kegg>.

**Accession numbers.** Microarray data are available in the ArrayExpress database (<http://www.ebi.ac.uk/arrayexpress>) under accession number E-MTAB-1821.

**MicroRNA target prediction.** Putative microRNAs targeting Hand2 were identified using the microRNA databases and target prediction tools miRBase (<http://microrna.sanger.ac.uk/>) and miRWalk (<http://www.umm.uni-heidelberg.de/apps/zmf/mirwalk/>)

**Representative images.** Representative images of whole hearts, histological sections and immunofluorescence pictures were successfully repeated at least three times; images of western and northern blots were successfully repeated at least two times.

**Statistical analysis.** The results are presented as mean  $\pm$  standard error of the mean (s.e.m.). Statistical analyses were performed using Prism software (GraphPad Software), and consisted of analysis of variance followed by Bonferroni's multiple comparison test when group differences were detected at the 5% significance level, or Student's *t*-test when comparing two experimental groups. Differences were considered significant when  $P < 0.05$ .

55. Morikawa, Y., D'Autreaux, F., Gershon, M. D. & Cserjesi, P. Hand2 determines the noradrenergic phenotype in the mouse sympathetic nervous system. *Dev. Biol.* **307**, 114–126 (2007).
56. Krutzfeldt, J. *et al.* Silencing of microRNAs *in vivo* with 'antagomirs'. *Nature* **438**, 685–689 (2005).
57. Lyakh, L., Ghosh, P. & Rice, N. R. Expression of NFAT-family proteins in normal human T cells. *Mol. Cell Biol.* **17**, 2475–2484 (1997).
58. Wilkinson, D. G., Bailes, J. A., Champion, J. E. & McMahon, A. P. A molecular analysis of mouse development from 8 to 10 days post coitum detects changes only in embryonic globin expression. *Development* **99**, 493–500 (1987).
59. De Windt, L. J., Lim, H. W., Haq, S., Force, T. & Molkentin, J. D. Calcineurin promotes protein kinase C and c-Jun NH2-terminal kinase activation in the heart. Cross-talk between cardiac hypertrophic signaling pathways. *J. Biol. Chem.* **275**, 13571–13579 (2000).
60. Van Oort, R. J. *et al.* MEF2 activates a genetic program promoting chamber dilation and contractile dysfunction in calcineurin-induced heart failure. *Circulation* **114**, 298–308 (2006).
61. Liang, Q. *et al.* The transcription factors GATA4 and GATA6 regulate cardiomyocyte hypertrophy *in vitro* and *in vivo*. *J. Biol. Chem.* **276**, 30245–30253 (2001).
62. Van Rooij, E. *et al.* Requirement of nuclear factor of activated T-cells in calcineurin-mediated cardiomyocyte hypertrophy. *J. Biol. Chem.* **277**, 48617–48626 (2002).
63. Armand, A. S. *et al.* Cooperative synergy between NFAT and MyoD regulates myogenin expression and myogenesis. *J. Biol. Chem.* **283**, 29004–29010 (2008).
64. Luo, C. *et al.* Recombinant NFAT1 (NFATp) is regulated by calcineurin in T cells and mediates transcription of several cytokine genes. *Mol. Cell Biol.* **16**, 3955–3966 (1996).

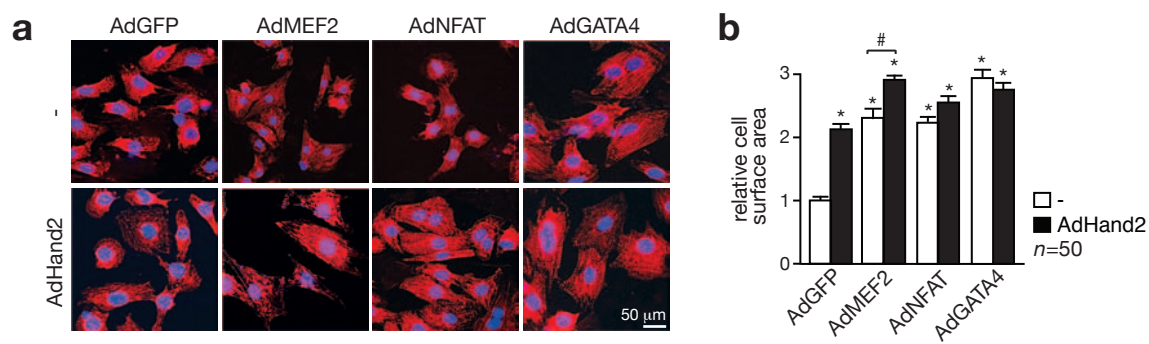


**Figure S1** Additive cardiomyocyte hypertrophy by Hand2 overexpression in combination with overexpression with MEF2, NFAT or GATA4. **(a)** Confocal microscopy images of neonatal rat cardiomyocytes infected with AdGFP, AdMEF2A, AdNFAT or AdGATA4 alone (top row). Confocal microscopy images of neonatal rat cardiomyocyte pre-infected with AdHand2 and infected with AdGFP, AdMEF2A, AdNFAT or AdGATA4

(bottom row). Nuclei were visualized with DAPI and cells were stained with an antibody against  $\alpha$ -actinin (red). Scale bar, 50  $\mu$ m. **(b)** Quantification of cell surface area in conditions in **(a)**,  $n$  refers to number of microscopic fields. \* $P < 0.05$  vs control group; # $P < 0.05$  vs experimental group (error bars are s.e.m.). Source data are shown in Supplementary Table S9.

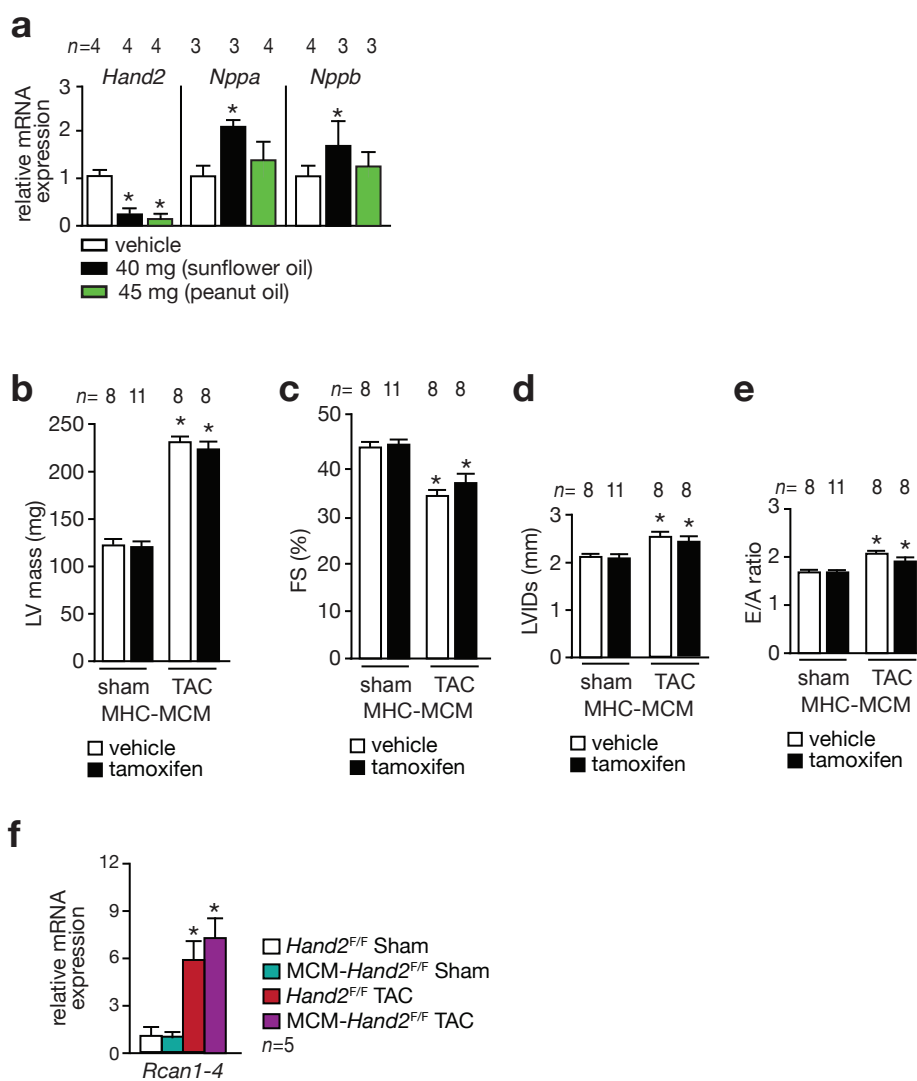


**Figure S2** Effect of tamoxifen treatment on cardiac function. **(a)** Real-time PCR analysis of *Hand2*, *Nppa* and *Nppb* transcript abundance in hearts from MHC-MerCreMer transgenic (MHC-MCM) mice treated with vehicle or tamoxifen at a dose of 40 mg/kg/day for 5 consecutive days dissolved in sunflower oil as described previously,<sup>36,37</sup> or tamoxifen at a dose of 45 mg/kg/day for 5 consecutive days dissolved in peanut oil (this study), *n* refers to number of hearts. **(b)** Quantification of the left ventricular mass, **(c)** fractional shortening (FS), **(d)** left ventricular internal diameter in systole (LVIDs) and **(e)**

E/A ratio from pulsed-wave Doppler imaging of the ratio of blood flow through the mitral valve during early (E) versus late (A) diastole in MHC-MCM mice, injected with vehicle (PBS) or 45 mg/kg/day tamoxifen dissolved in peanut oil, *n* refers to number of animals. **(f)** Real-time PCR analysis of *Rcan1.4* expression in hearts from mice with indicated genotype, pre-treated with vehicle or tamoxifen and subjected to sham or TAC surgery, *n* refers to number of hearts. \**P* < 0.05 vs control group; #*P* < 0.05 vs experimental group (error bars are s.e.m.). Source data are shown in Supplementary Table S9.

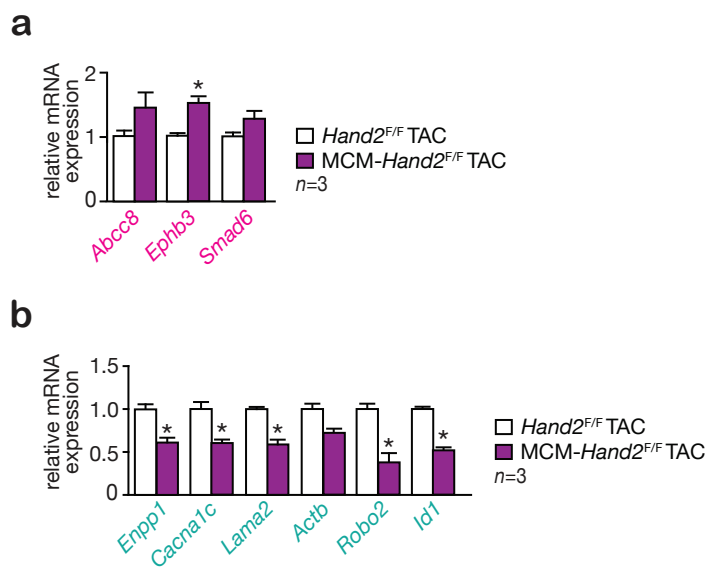


**Figure S3** Real-time PCR validation of microarray results in pressure overloaded *Hand2*<sup>F/F</sup> and MCM-*Hand2*<sup>F/F</sup> mice. **(a)** Validation of the gene profiling microarray results from Supplementary **Tables S1** and **S2** by quantitative real-time PCR, *n* refers to number of hearts. Relative mRNA expression levels were determined for transcripts that were increased in

expression in pressure overloaded *Hand2*-deficient hearts (*Abcc8*, *Ephb3*, *Smad6*) or **(b)** downregulated in pressure overloaded *Hand2*-deficient hearts (*Enpp1*, *Cacna1c*, *Lama2*, *Actb*, *Robo2* and *Id1*), *n* refers to number of hearts. \**P* < 0.05 vs control group (error bars are s.e.m.). Source data are shown in Supplementary Table S9.

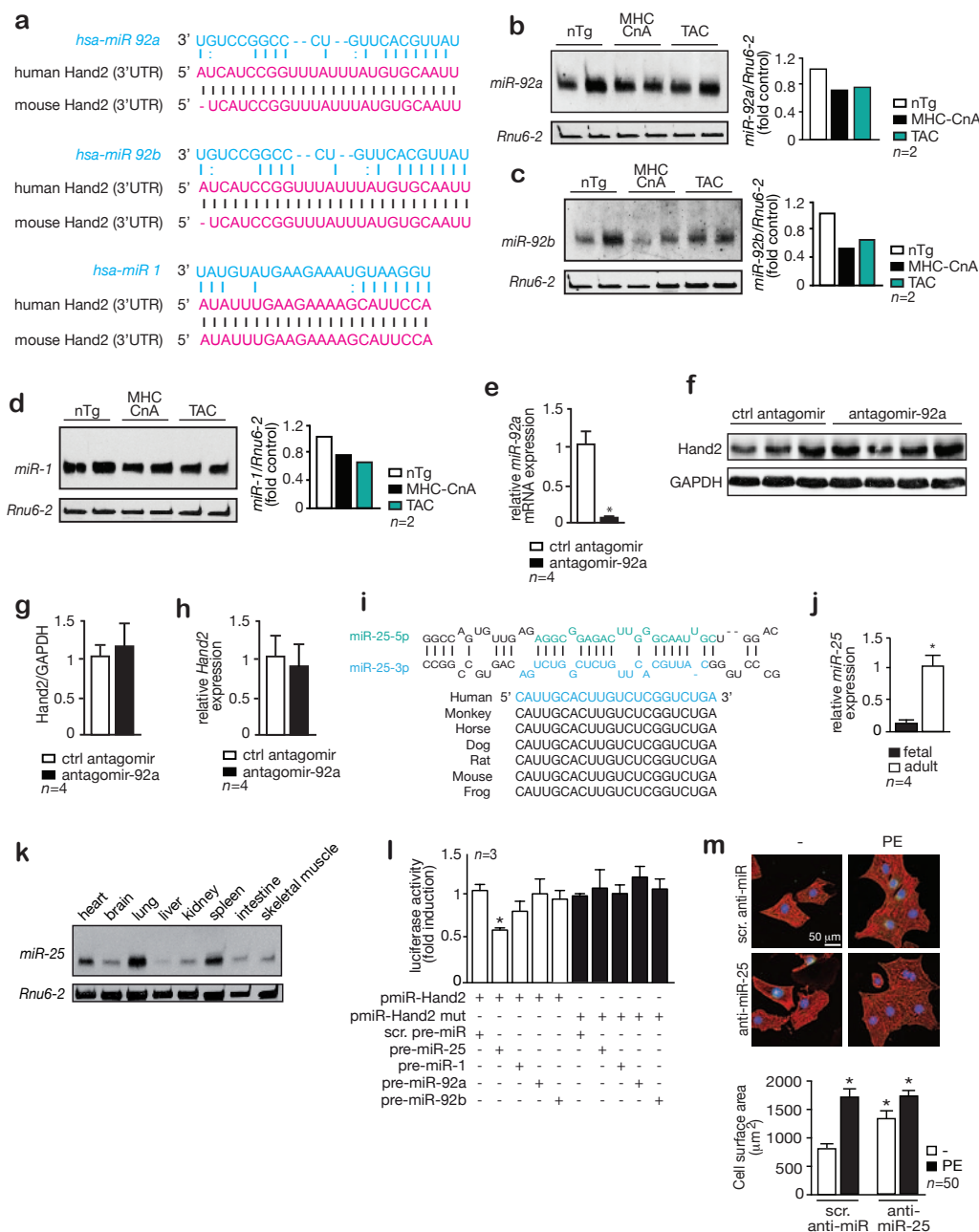


**Figure S4** miR-25, miR-92a, miR-92b and miR-1 expression levels in heart disease. **(a)** Location of potential *miR-92a*, *miR-92b* and *miR-1* seed regions in human and mouse *Hand2* 3'UTR. **(b)** Northern blot analysis of *miR-92a* expression in hearts from nontransgenic littermates (nTg), calcineurin transgenic mice (MHC-CnA) and mice subjected to transverse aortic constriction (TAC). Quantification of *Rnu6-2* corrected Northern blot signals for *miR-92a* (right panel), *n* refers to number of hearts. **(c)** Northern blot analysis of *miR-92b* expression in hearts from nontransgenic littermates (nTg), calcineurin transgenic mice (MHC-CnA) and mice subjected to transverse aortic constriction (TAC). Quantification of *Rnu6-2* corrected northern blot *miR-92b* signals (right panel), *n* refers to number of hearts. **(d)** Northern blot analysis of *miR-1* expression levels in hearts from nTg mice, MHC-CnA mice and mice subjected to TAC. Quantification of *Rnu6-2* corrected Northern blot *miR-1* signals (right panel), *n* refers to number of hearts. **(e)** Real-time PCR analysis of *miR-92a* expression in hearts from mice treated with scrambled antagomir (ctrl antagomir) or antagomir specific for *miR-92a* (antagomir-92a), *n* refers to number of hearts. **(f)** Western blot analysis of endogenous Hand2 or GAPDH protein expression in hearts from mice treated with ctrl antagomir

or antagomir-92a. **(g)** Quantification of GAPDH corrected Hand2 Western blot signals from **(f)**, *n* refers to number of hearts. **(h)** Real-time PCR analysis of *Hand2* transcript abundance in hearts from mice treated with ctrl antagomir or antagomir-92a, *n* refers to number of hearts. **(i)** Schematic representation of the precursor sequence of *hsa-miR-25* and conservation level of the mature *miR-25-3p* strand. **(j)** Endogenous *miR-25* expression in human fetal myocardium and human adult myocardium indicating a higher expression level of miR-25 in the adult human heart, *n* refers to number of hearts. **(k)** Northern blot analysis of *miR-25* expression in multiple mouse organs. **(l)** Activity assay of luciferase reporter construct harboring an intact or mutated Hand2 3'UTR after transfection with premiR-25, pre-miR-92a, pre-miR-92b or pre-miR-1 in neonatal rat cardiomyocytes. A scrambled precursor miR (scr.pre-miR) was used as a control, *n* refers to number of transfection experiments. **(m)** Confocal microscopy images of neonatal rat cardiomyocytes transfected with scrambled anti-miR (scr.anti-miR) or anti-miR for *miR-25* (anti-miR-25) and treated with PE for 24 h. Quantification of cell surface areas from these conditions (lower panel), *n* refers to number of microscopic fields. \**P* < 0.05 vs control group (error bars are s.e.m.). Source data are shown in Supplementary Table S9.

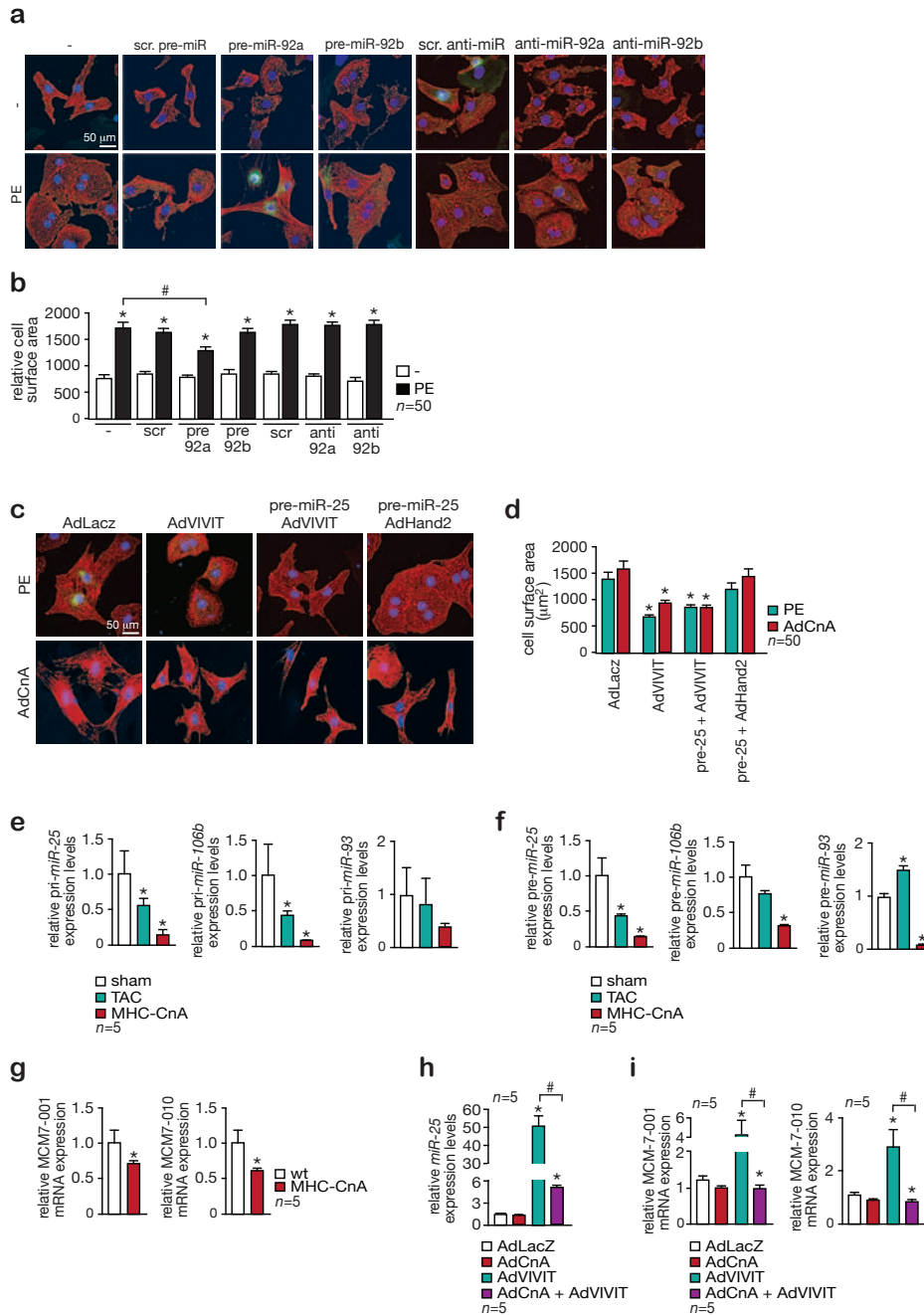


**Figure S5** Downregulation of the *miR-106b~25* cluster in the adult heart involves NFAT-dependent transcriptional repression. **(a)** Confocal microscopy images of neonatal rat cardiomyocytes transfected with scrambled precursor (scr.pre-miR), synthetic precursor scrambled anti-miR (scr.anti-miR) or anti-miR for *miR-92a* (pre-miR-92a, anti-miR-92a), *miR-92b* (pre-miR-92b, anti-miR-92b) and treated with or without PE for 24 h. Scale bar, 50  $\mu$ m. **(b)** Quantification of cell surface areas from conditions in **(a)**, *n* refers to number of microscopic fields. **(c)** Confocal microscopy images of neonatal rat cardiomyocytes infected with AdLacZ (control adenovirus), AdVIVIT (adenovirus overexpressing the VIVIT optimized NFAT inhibitory peptide), AdVIVIT + pre-miR-25 and AdHand2 + pre-miR-25. In all conditions cells were treated with PE or AdCnA for 24 h. Scale bar, 50  $\mu$ m. **(d)** Quantification of cell surface areas from conditions in **(c)**, *n* refers to number of microscopic fields. **(e)**

Pri-miR-25, pri-miR-106b and pri-miR-93 are down-regulated in two animal models of heart failure: TAC hearts and MHC-CnA Tg hearts, *n* refers to number of hearts. **(f)** Pre-miR-25, pre-miR-106b and pre-miR-93 are downregulated in two animal models of heart failure: TAC hearts and MHC-CnA Tg hearts, *n* refers to number of hearts. **(g)** Real-time PCR analysis of the MCM7-001 and MCM7-010 transcripts in wild-type (wt) versus MHC-CnA Tg hearts, *n* refers to number of hearts. **(h)** Real-time PCR analysis of *miR-25* expression of neonatal rat cardiomyocytes infected with AdLacZ, AdCnA, AdVIVIT, and AdCnA with AdVIVIT, *n* refers to number of dishes. **(i)** Real-time PCR analysis of MCM7-001 and MCM7-010 expression of neonatal rat cardiomyocytes infected with AdLacZ, AdCnA, AdVIVIT, and AdCnA with AdVIVIT, *n* refers to number of dishes. \**P* < 0.05 vs control group; #*P* < 0.05 vs experimental group (error bars are s.e.m.). Source data are shown in Supplementary Table S9.

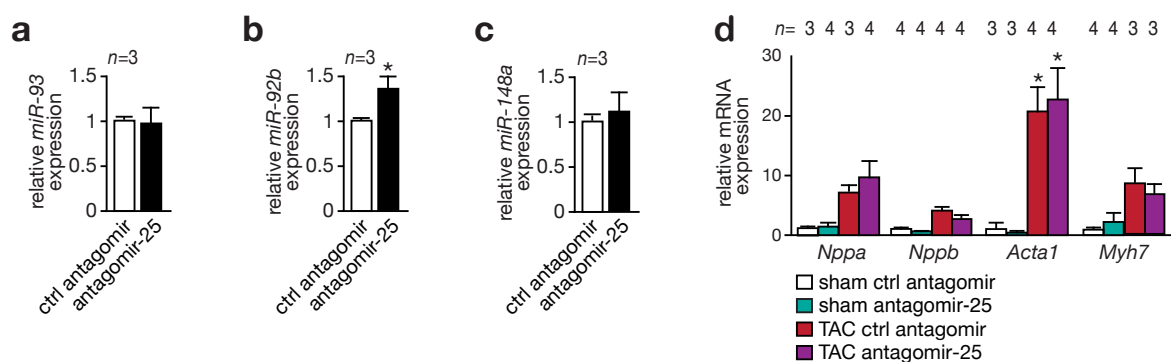


**Figure S6** Specific *miR-25* silencing with antagomir-25. **(a)** Real-time PCR analysis of *miR-93* expression in hearts from mice receiving control (ctrl) antagomir or antagomir against *miR-25* (antagomir-25) and subjected to sham or transverse aortic constriction (TAC) surgery, *n* refers to number of hearts. **(b)** Real-time PCR analysis of *miR-92b* expression in hearts from mice receiving control (ctrl) antagomir or antagomir against *miR-25* and subjected to sham or transverse aortic constriction (TAC) surgery, *n* refers to number of hearts. **(c)** Real-time PCR analysis of *miR-148a*

expression in hearts from mice receiving control (ctrl) antagomir or antagomir against *miR-25* and subjected to sham or transverse aortic constriction (TAC) surgery, *n* refers to number of hearts. **(d)** Real-time PCR analysis of relative transcript abundance for the fetal marker genes *Nppa*, *Nppb*, *Acta1* and *Myh7* in hearts from mice treated with ctrl antagomir or antagomir-25 following sham or TAC surgery, *n* refers to number of hearts. \* $P < 0.05$  vs control group (error bars are s.e.m.). Source data are shown in Supplementary Table S9.

